

Seismic Tomography 2024

Andreas Fichtner¹, Brian L. N. Kennett², Victor C. Tsai³, Clifford H. Thurber⁴, Arthur J. Rodgers⁵, Carl Tape⁶, Nicholas Rawlinson⁷, Roger D. Borchardt⁸, Sergei Lebedev⁷, Keith Priestley⁷, Christina Morency⁵, Ebru Bozdogan⁹, Jeroen Tromp¹⁰, Jeroen Ritsema¹¹, Barbara Romanowicz¹², Qinya Liu¹³, Eva Golos⁴, and Fan-Chi Lin¹⁴

ABSTRACT

Seismic tomography is the most abundant source of information about the internal structure of the Earth at scales ranging from a few meters to thousands of kilometers. It constrains the properties of active volcanoes, earthquake fault zones, deep reservoirs and storage sites, glaciers and ice sheets, or the entire globe. It contributes to outstanding societal problems related to natural hazards, resource exploration, underground storage, and many more. The recent advances in seismic tomography are being translated to nondestructive testing, medical ultrasound, and helioseismology. Nearly 50 yr after its first successful applications, this article offers a snapshot of modern seismic tomography. Focused on major challenges and particularly promising research directions, it is intended to guide both Earth science professionals and early-career scientists. The individual contributions by the coauthors provide diverse perspectives on topics that may at first seem disconnected but are closely tied together by a few coherent threads: multiparameter inversion for properties related to dynamic processes, data quality, and geographic coverage, uncertainty quantification that is useful for geologic interpretation, new formulations of tomographic inverse problems that address concrete geologic questions more directly, and the presentation and quantitative comparison of tomographic models. It remains to be seen which of these problems will be considered solved, solved to some extent, or practically unsolvable over the next decade.

KEY POINTS

- This Special Issue introduction documents opinions on major challenges and promising research directions.
- Although no efforts were made to align these opinions, a small number of topics emerged as outstanding issues.
- This article is intended to be a resource for both established and early-career scientists.

INTRODUCTION

Seismic tomography is the art of translating recordings of seismic waves into quantitative images of the Earth's interior. Conceptualized nearly 50 yr ago (e.g., Aki and Lee, 1976; Aki *et al.*, 1977; Dziewoński *et al.*, 1977), the family of seismic tomography methods has grown and diversified rapidly, thereby evolving into one of the cornerstones of geoscience. Seismic tomography reveals the dynamics and composition of the Earth and other planetary bodies, illuminates the structure of active volcanoes and fault zones, constrains the internal flow patterns of glaciers and ice sheets, provides information on deep reservoirs and storage sites, and enables the accurate simulation of earthquake-induced ground motion, to list just a few of its most prominent uses.

This broad impact of modern seismic tomography is rooted in a long series of developments that produce Earth models

with continuously improving spatial resolution and increasingly tighter constraints on seismic properties that are closely

1. Department of Earth Sciences, ETH Zurich, Zürich, Switzerland, <https://orcid.org/0000-0003-3090-963X> (AF); 2. Research School of Earth Sciences, The Australian National University, Canberra, Australia, <https://orcid.org/0000-0003-2206-5350> (BLNK); 3. Department of Earth, Environmental and Planetary Sciences, Brown University, Providence, Rhode Island, U.S.A., <https://orcid.org/0000-0003-1809-6672> (VCT); 4. Department of Geoscience, University of Wisconsin-Madison, Madison, Wisconsin, U.S.A., <https://orcid.org/0000-0002-4940-4618> (CHT); <https://orcid.org/0000-0002-7320-2493> (EG); 5. Lawrence Livermore National Laboratory, Livermore, California, U.S.A., <https://orcid.org/0000-0002-6784-5695> (AJR); <https://orcid.org/0000-0002-9154-5596> (CM); 6. University of Alaska Fairbanks, Fairbanks, Alaska, U.S.A., <https://orcid.org/0000-0003-2804-7137> (CT); 7. Department of Earth Sciences, University of Cambridge, Cambridge, United Kingdom, <https://orcid.org/0000-0002-6977-291X> (NR); <https://orcid.org/0000-0003-0004-5009> (SL); <https://orcid.org/0000-0001-6515-1318> (KP); 8. U. S. Geological Survey, Menlo Park, California, U.S.A., <https://orcid.org/0000-0002-8668-0849> (RDB); 9. Department of Applied Mathematics and Statistics and Department of Geophysics, Colorado School of Mines, Golden, Colorado, U.S.A.; 10. Department of Geosciences and Program in Applied and Computational Mathematics, Princeton University, Princeton, New Jersey, U.S.A.; 11. Earth and Environmental Sciences, University of Michigan, Ann Arbor, Michigan, U.S.A.; 12. Department of Earth and Planetary Science, University of California at Berkeley, Berkeley, California, U.S.A.; 13. Department of Physics and Department of Earth Sciences, University of Toronto, Toronto, Canada, <https://orcid.org/0000-0002-1071-2314> (QL); 14. Department of Geology and Geophysics, University of Utah, Salt Lake City, Utah, U.S.A., <https://orcid.org/0000-0003-0394-6830> (F-CL)

*Corresponding author: andreas.fichtner@erdw.ethz.ch

Cite this article as Fichtner, A., B. L. N. Kennett, V. C. Tsai, C. H. Thurber, A. J. Rodgers, C. Tape, N. Rawlinson, R. D. Borchardt, S. Lebedev, K. Priestley, *et al.* (2024). Seismic Tomography 2024, *Bull. Seismol. Soc. Am.* **XX**, 1–29, doi: [10.1785/0120230229](https://doi.org/10.1785/0120230229)

© Seismological Society of America

related to dynamic processes such as attenuation, anisotropy, poroelasticity, or the topography of internal discontinuities. Most of these developments, traced in several books and review articles (e.g., Iyer and Hirahara, 1993; Nolet, 2008; Fichtner, 2010; Liu and Gu, 2012; Ringler *et al.*, 2022), fall into one of four categories: (1) improvements in data coverage and quality, often related to novel instrumentation; (2) reductions of forward and inverse modeling errors through theoretical and numerical advances; (3) innovative data processing methods, including methods to extract targeted information from seismic data; and (4) the exploitation of increased computational power and novel hardware.

Despite the success and maturity of seismic tomography, our knowledge still requires substantial improvements to address both academic questions concerning the thermochemical state of the Earth and burning societal needs. The latter relate, for instance, to earthquake and volcanic hazards, geothermal energy exploration and production, long-term underground storage of hazardous materials and energy sources, as well as natural resource exploration and management.

Within this context, the most pertinent challenges and the most promising research directions in seismic tomography were chosen to be the focus of a dedicated meeting organized by the Seismological Society of America that took place on October 2022 in Toronto, Canada. This introductory article to the BSSA Special Section on *Modern Seismic Tomography* is a condensate of the Toronto meeting. It portrays the state of the art and contains opinions by long-term practitioners and developers on what the outstanding challenges and exciting topics for the next decade should be. They include complete reformulations of seismic tomography, multiparameter inversion of more diverse datasets, uncertainty quantification and fundamental limitations of tomography, as well as advances and recommendations on Earth model presentation and interpretation. The content is deliberately unfiltered to ensure that potentially different opinions can be represented. Rather than offering a discussion or review, the text is intended to provoke discussions and critical reflections.

The contributions to this BSSA Special Section explore many of the directions covered in this opinion article. Proposals of novel forward and inverse modeling approaches, for example, can be found in the works of Borchardt (2024), Del Piccolo *et al.* (2024), and Lebedev *et al.* (2024). Lebedev *et al.* (2024) implement seismic thermography by making plausible assumptions on mantle composition and extracting information from noisy surface-wave data to directly constrain temperature variations. Del Piccolo *et al.* (2024) extend trans-dimensional tomography to imaging anisotropy in the upper mantle, thereby quantifying the delicate balance between increasing model uncertainties and the need to incorporate additional parameters to describe anisotropic velocity variations. Borchardt (2024) reviews exact viscoelastic raytracing algorithms that quantify ray trajectory perturbations across

anelastic boundaries and effects of anelasticity on seismic tomography models.

Two of the contributions are concerned with the construction of multiscale seismic Earth models. Lyu *et al.* (2024) introduce a numerical wave propagation approach for accurately coupling highly resolved local domains and lower-resolution global-scale models in the context of box tomography. This is complemented by the work of Zhou *et al.* (2024), who propose a method for seismic velocity model fusion based on a probability graph method that avoids the introduction of artifacts and the suppression of small-scale structure.

Several articles exploit either very large data volumes or newly collected data to make concrete inferences about Earth structure and dynamics. Using ambient noise tomography, Lv *et al.* (2024) suggest that midlower crustal flow and northeast subduction of the Indian plate control deformation of the eastern Himalayan syntaxis, which is the leading edge of the Indian–Asian collision. Mahesh *et al.* (2024) image the Andaman and Nicobar subduction zone using ocean-bottom seismometer data, and reveal mantle upwellings as well as volcanism-related low-velocity regions. Civiero *et al.* (2024) employed over 1.17 million Rayleigh and 300,000 Love-wave fundamental mode phase-velocity measurements in the 17–310 s period range to constrain 1D upper-mantle models averaged over the globe and for eight distinct tectonic environments. One of the robust features is a distinct flip in the sign of global radial anisotropy from positive ($V_{SH} > V_{SV}$) to negative at 200–300 km depth.

Three novel full-waveform inversion (FWI) models complete this Special Section. Carmona *et al.* (2024) extracted frequency-dependent phase and amplitude information to constrain wave-speeds and shear attenuation beneath the Arabian plate, thereby shedding light onto the origin of Cenozoic volcanism in the western Arabian Peninsula. Partly overlapping with their study region, Rodgers *et al.* (2024) present a radially anisotropic model of the Middle East and southwest Asia. The model constrains numerous regional tectonic features, and is shown to be sufficiently robust to help improve earthquake hazard analyses and explosion monitoring. Last but not the least, Thrastarson *et al.* (2024) combine stochastic minibatch optimization and wave-field-adapted spectral-element meshes to reduce the computational cost of a quasi-Newton iteration by more than two orders of magnitude compared to standard FWI. This drastic cost reduction enables the inversion of more than 6 million three-component waveform recordings from 2366 earthquakes, leading to their final global-scale model REVEAL.

This introductory article is organized as a sequence of short contributions, each written by one of the coauthors on one or several topics that they find most relevant or challenging. As far as possible, the contributions are ordered and loosely grouped according to their particular focus. In the final section, we attempt to summarize some coherent threads that emerge, despite the remarkable diversity of the contributions.

INFERENCE, DATA QUALITY, AND ALTERNATIVES (Victor C. Tsai)

In my view, the most important directions for the future of seismic tomography are (1) to frame tomography to be better able to make clear, robust inferences about the Earth's interior in a practically useful manner, (2) to improve data quality and quantity, and (3) to diversify the approaches, tools, and datasets used. Although other directions are still worthwhile to pursue, I believe it is of lesser importance to focus on areas such as the improved accuracy of synthetics, computational efficiency, and machine learning that are the current focus of many researchers.

Robust, practical inference from imaging

Given the limitations of geophysical data, the vast majority of tomographic results require significant smoothing or regularization to achieve unique answers (Jackson, 1972). One main reason for this is an implicit philosophy taken favoring flexible, mathematically convenient parameterizations such as grid cells, pixels, spherical harmonics, or splines. Unfortunately, due to the regularization, such flexible “discovery oriented” parameterizations do not achieve physically realistic results, and it is typically impossible to truly falsify any interpretations of features due to the qualitative nature of such interpretations. Because geophysical data will always be limited (even with progress in direction (2)), I suggest that the most progress would be made by making tomographic inversions more “inference oriented” by inverting for simplified but physically reasonable models for the geological structures of potential interest that are uniquely determined without regularization. Within such an inference framework, multiple alternative hypotheses could be tested by running multiple inversions and using a model selection process (Sambridge *et al.*, 2006; Vehtari *et al.*, 2017). This general practical inference direction is discussed in significantly more detail in Tsai (2023) and Tsai *et al.* (2023).

Data quality and quantity

The severe undersampling of information from the Earth's interior is partly due to data quality and quantity. Not only are there very few seismic stations in the oceans for obvious cost reasons, but there are also few openly accessible stations in Russia and Africa for various political and logistical reasons, leading to large areal coverage gaps (Incorporated Research Institutions for Seismology [IRIS], 2018). Improving this coverage is crucial for deep Earth tomography to yield useful constraints. Equally importantly, however, is data quality. Unfortunately there has been the recent trend toward cheaper and lower quality seismic stations due to interest in differential measurements (and also with the hope that \sqrt{N} stacking can overcome the quality limitations). However, the abundant uncertainties and structural biases that arise due to low-quality station installations and instruments often prevent tomographers from understanding which uncertainties are “true”

uncertainties related to deep Earth structure and which are due to local (sometimes extremely local) site issues, making the observations depart significantly from the typically assumed weakly attenuating elastic Earth.

Diversification of approaches and data types

Although many researchers would argue that convergence to standard methodologies and datasets is a useful goal, there is a danger of overreliance on a standard set of tools and data. In global tomography, much fanfare has been given to the fact that many global mantle models are starting to agree on certain broad features of the deep mantle (Cottaar and Lekic, 2016). Although this is a major step forward from the previous generation of global tomographic models, an important question is how much of this agreement is related to using similar datasets and similar methodologies. Currently, this question cannot be answered due to the significant overlap in all methodologies and data used for the compared models. This underscores the need for high-quality alternatives to standard approaches to utilizing the same data as well as novel datatypes that are truly independent of the seismic data. I advocate for alternatives to standard adjoint frameworks that are nonetheless physically and mathematically justified, for example, using frameworks where improvements in misfit are accomplished through different paths in model space (Haney and Tsai, 2015, 2017). For data types, although it is difficult for other data to achieve the resolution of seismic data, it will be crucial to test seismically inferred models of Earth's interior with neutrino (Donini *et al.*, 2019), muon (Tanaka *et al.*, 2009), electromagnetic (Naif *et al.*, 2013), gravity (Oldenburg, 1974), and geodetic (Park *et al.*, 2023) data that have different sensitivities and biases from the seismic data. Although joint inversions with multiple data types are becoming more popular, these do not help test the robustness of the obtained images. Truly independent data must be left out of prospective tests to ensure against data dredging problems (Nuzzo, 2014; Wasserstein and Lazar, 2016).

THE IMPORTANCE OF INVERTING FOR WHAT WE REALLY WANT TO KNOW (Sergei Lebedev)

What is the goal of seismic tomography? To yield inferences on the structure and dynamics of Earth, as most Earth scientists would see it. For some applications, such as earthquake source or ground-motion studies, models of the distribution of seismic velocities are what is needed. But for those concerned with Earth structure and dynamics, key properties of interest include temperature (T), composition, density, and movements of the rock at depth. Tomography is a quest for information to paraphrase Tarantola and Valette (1982). With tomography's goals in mind, it must be a quest for information on what we want to know (T , etc.). This is a perilous quest with treacherous pitfalls. Settle for a nonunique model half-way, build inferences on its poorly constrained features, and end up with implausible results and all useful information lost.

We can avoid losing information in the nonuniqueness of intermediate solutions by establishing direct quantitative relationships between the data and the inferences of interest (see also [Tsai et al., 2023](#)). Inverting seismic data directly for temperature and density, or temperature and composition, has been discussed in the field for decades. Yet, implementing this approach has challenges, and the field has generally stuck with the tried-and-tested one instead: let us not risk increasing errors by introducing potentially uncertain temperature–wave-speed relationships; let us do what we know well and build the best possible seismic-velocity models. The concerns are valid, and solving for T and, so forth, is not straightforward. Yet, the consequences of not inverting for what we really want to know are the loss of information from seismic data, failure to incorporate relevant information from other data types, and other setbacks in our quest for information.

New opportunities

Tomography has come a long way in its 40 + yr. In the early days, important discoveries were made by qualitative interpretation of seismic-velocity anomalies mapped by the models. Since then, the seismic data sampling of the Earth has increased dramatically. Whereas the first global tomographic models were computed using hundreds of seismograms, the recent ones are using hundreds of thousands and millions of them. Is tomography's discovery potential reaching saturation? For qualitative interpretation of larger-scale features: Yes, in many cases. For quantitative inferences: No, quite the opposite. The growth in the data sampling and progress in computational petrology and other relevant fields are now giving us a new ability: to resolve quantitatively what we want to know.

What to do?

1. Thermodynamic inversion: Computational petrology gives us the means to quantitatively relate temperature and composition at depth to elastic parameters (e.g., [Connolly, 2005](#)) and then to seismic observables (e.g., [Fullea et al., 2012](#)). This solves the forward problem. The corresponding inverse problem is nonlinear. Posing and solving it for large datasets is an outstanding challenge. One approach for upper-mantle thermochemical imaging, for example, is to obtain a phase-velocity model for the region or the globe and, then, invert the Love and Rayleigh phase-velocity curves for temperature and composition, point by point (e.g., [Fullea et al., 2021](#); [Lebedev et al., 2023](#)). The nonlinear inverse problem for every column is small, and can be solved readily and with exhaustive uncertainty analysis where needed.
2. Seismic thermography: Thermodynamic inversion can not only bring in extra nonseismic information on what we want to know but also helps us extract information from seismic data more fully and more accurately. A priori knowledge, such as the shapes of plausible lithospheric geotherms, reduces the nonuniqueness of the problem and

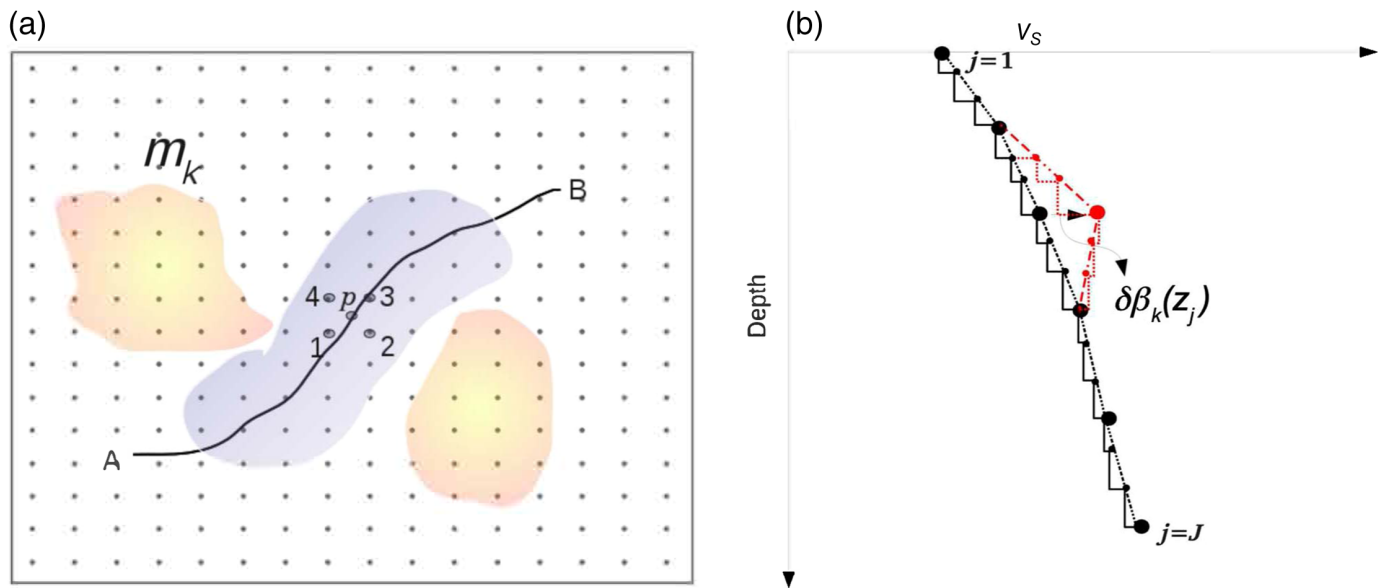
steers the inversion to the physically plausible solutions within the broad misfit valleys in the model space. Because of the much greater sensitivity of seismic data to temperature than to composition, we can invert seismic data directly for temperature, with reasonable assumptions on composition and other relevant properties, and with additional inversion parameters such as anisotropy. This amounts to Seismic Thermography of the Earth ([Lebedev et al., 2024](#)).

3. A priori information: The optimal resolution tomography of [Bonadio et al. \(2021\)](#) shows an example of an effective use of seismic a priori information, in this case, to solve the Backus–Gilbert problem ([Backus and Gilbert, 1970](#)) as applied to surface-wave tomography. We know that the phase-velocity curve at a point must be smooth due to the inherent properties of the data. The roughness on the curves extracted from a set of phase-velocity maps thus gives us a direct estimate of the model error and a way to solve the Backus–Gilbert problem (finding an optimal resolving length at every point, defined as the narrowest one such that the model error at the point is under a threshold).
4. Errors: The largest uncertainty in 1D or 3D seismic-velocity models is normally due to parameter trade-offs. Covariance and resolution matrices can be computed, but they do not quantify directly the uncertainty of our inferences. Model-space projection ([Bartzsch et al., 2011](#); [Lebedev et al., 2013](#)) can be easily applied to smaller inverse problems and quantify the uncertainty of what we really want to know, for example, the lithospheric thickness or asthenospheric temperature.

JOINT INVERSION OF BODY AND SURFACE WAVES (Clifford H. Thurber)

Two end members of seismic tomography are body-wave arrival-time tomography and full-waveform tomography. Arrival-time tomography can be thought of as an infinite-frequency approach, whereas full-waveform tomography exploits a broadband of frequencies in fitting selected portions of seismograms. Lying somewhat in between these schemes are normal-mode and surface-wave tomography that can again exploit broadband signals but employ parametric inversions as used for arrival-time work.

Arrival-time tomography was developed in the mid-1970s in a series of articles by Keiiti Aki and coworkers on local- and regional-scale imaging ([Aki and Lee, 1976](#); [Aki et al., 1977](#)), and has since been exploited in many different ways with a variety of inversion algorithms. Tomography exploiting normal modes and surface waves emerged in the mid-1980s in articles mainly by Adam Dziewoński and coworkers on global-scale tomography ([Dziewoński, 1984](#); [Dziewoński and Anderson, 1984](#); [Woodhouse and Dziewoński, 1984](#)). Over the past several decades, a variety of full-waveform



tomography methods have been developed and applied to seismic imaging problems over a wide range of scales (Tromp, 2020), a notable example being SPEC-FEM3D (Komatitsch and Vilotte, 1998; Komatitsch and Tromp, 1999).

Full-waveform tomography is arguably the most powerful current approach to seismic imaging, but, in practice, its high-computational demands tend to limit the model domain size, spatial resolution, and/or period range. An option for imaging with moderate resource demands is joint body-wave and surface-wave tomography (JBST), whereby both the arrival times of body-wave phases and the dispersion characteristics of surface waves are jointly exploited. In this way, more of the content of seismograms can be utilized to constrain both P - and S -wavespeed distributions, and often a broader period range is employed than is feasible with FWI.

Two codes implementing JBST are by Fang et al. (2016), *jointTomoBS*, built on *tomoDD* (Zhang and Thurber, 2003) and by Eberhart-Phillips and Fry (2017), *simul2017*, built on *simul2000* (Thurber and Eberhart-Phillips, 1999). The treatment of P waves is virtually the same in the two codes, but the way that S wave and surface-wave data are used differs between the two methods, and also the calculation of sensitivities and the matrix inversion strategies differ. For Fang et al. (2016), S -wave arrival times and interstation surface-wave group and/or phase travel times between station pairs over a range of periods are used, and an approximate conjugate gradient method is employed for the matrix inversion. For Fang et al. (2016), residuals are simply the difference between an observed and the corresponding calculated interstation group or phase travel time at a given period, and sensitivities for the matrix inversion are calculated somewhat analogously to body-wave sensitivities in terms of a wavepath horizontally through the corresponding 2D group velocity map, with local 1-D sensitivity for each “column” of surrounding nodes vertically (Fig. 1). In contrast, Eberhart-Phillips and Fry (2017) use

Figure 1. Illustration of the Fang et al. (2016) model discretization. (a) Horizontal plane: The black solid line represents the propagation path between two stations A and B for the surface wave at some period. The phase slowness at any point p along the path is determined from the values at four surrounding horizontal grid points (1–4) using bilinear interpolation. (b) Vertical direction: The vertical grid model (bigger black dots with finer layers shown as the black line) is perturbed (as shown by the red dot and red dashed lines) to compute the depth sensitivity of dispersion data to model parameters via differences. Modified from Fang et al. (2016). The color version of this figure is available only in the electronic edition.

S – P times and 2D surface-wave group velocity maps for a range of periods, and a more accurate matrix inversion method (Cholesky decomposition) is used in conjunction with the hypocenter-velocity model parameter separation step (Pavlis and Booker, 1980; Spencer and Gubbins, 1980). In this case, residuals are evaluated between a group velocity value at a point in the 2D velocity map (yellow star in Fig. 2) and the predicted value based on a 1D average of velocities in a box centered on the selected point (red circles in Fig. 2). The width and depth extent of the box increases with increasing period. The sensitivities at all the points in the box are computed using the group velocity sensitivity kernels from the average 1D model for V_P and V_S , with V_S related to V_P and V_P/V_S .

Although these approaches to joint body-wave and surface-wave tomography are clearly a simplification and approximation compared to full-waveform tomography, they have the advantages of combining the complementary sampling characteristics of Earth structure by body waves versus surface waves, the potential for finer-scale resolution with higher-frequency data, and the method’s computational efficiency.

One area for the future work on further reducing the gap between such joint body-wave and surface-wave methods and full-waveform tomography is in improving the evaluation of sensitivities. The use of finite-frequency kernels (Marquering

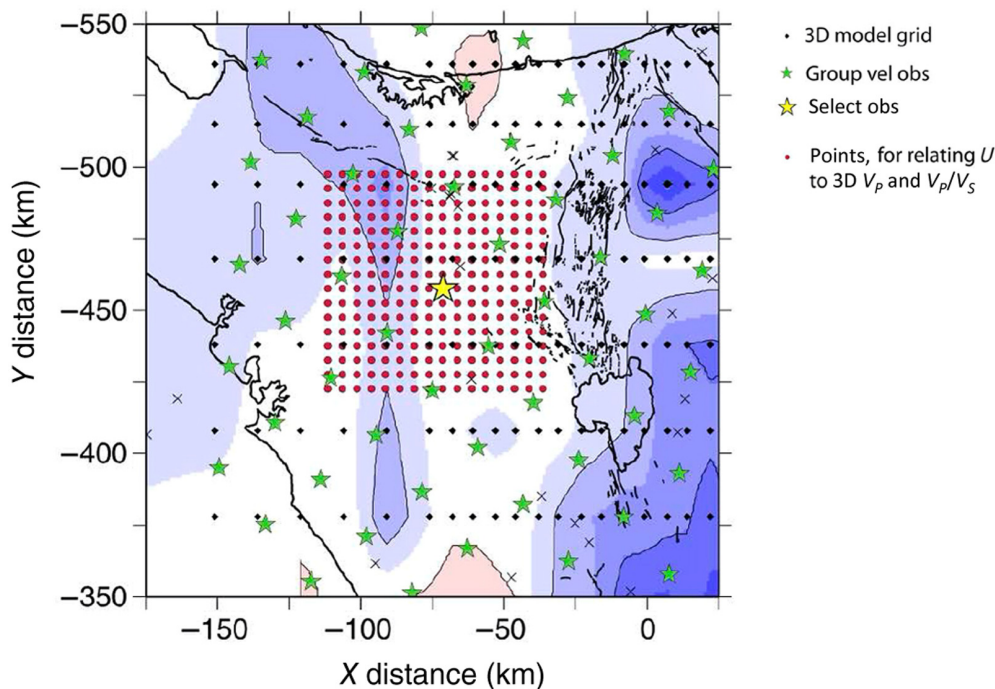


Figure 2. Map view of part of a velocity grid across New Zealand showing an example of the box for computing group velocity (U) partial derivatives at points (red dots) in a volume surrounding a U observation (yellow star) analogous to points along a path from an earthquake travel time. Small dots are 3D velocity grid nodes; stars are U observation locations (nodes of U velocity map). From Eberhart-Phillips and Fry (2017). The color version of this figure is available only in the electronic edition.

et al., 1999; Dahlen *et al.*, 2000; Zhao *et al.*, 2000; Tromp *et al.*, 2005) for both body waves and surface waves appears to be the most logical target. The increased computational burden may be tractable with the use of adjoint methods. The computational tools for achieving this are generally available, including some recent “specialized” techniques. Among the latter are double-difference adjoint seismic tomography (Yuan *et al.*, 2016), sensitivity kernels for multicomponent ambient noise empirical Green’s functions (Wang *et al.*, 2019), and sensitivity kernels for differential travel-time measurements using a three-station approach (Liu, 2020).

SEISMIC TOMOGRAPHY AND INSIGHT INTO MANTLE PROPERTIES (Keith Priestley)

In seismic tomography research, there has always been the impulse to develop more accurate tomographic methods to eliminate simplifying approximations. For example, most tomography with surface waves employs the great-circle approximation (e.g., Woodhouse and Dziewoński, 1984; Ekström and Dziewoński, 1998; Lebedev and Nolet, 2003; Debayle and Ricard, 2012), even though this does not permit resolution of structures smaller than their sensitivity zone (e.g., Spetzler and Snieder, 2001; Yoshizawa and Kennett, 2002). Further improvement in resolution is being sought through utilizing more accurate forward calculations and adjoint

tomography (e.g., Komatitsch and Tromp, 2002; Fichtner *et al.*, 2006). Although this is clearly the way forward, it is computationally intense and, at present, is limited in the number of seismic waveforms that can be inverted. The computational overhead will ease with future increases in computational power, but those increases will also require more efficient algorithms (e.g., Capdeville *et al.*, 2002; van Herwaarden *et al.*, 2020).

More complete subsurface tomographic imaging requires inverting waveforms whose various arrivals are sensitive to different parts of the Earth. To maximize the amount of information extracted from a waveform, a misfit function is required that permits retrieving information from low-amplitude phases in the presence of large amplitude phases—an active area of

research, especially in the seismic exploration community (Virieux *et al.*, 2017; Yang and Engquist, 2018; Plady *et al.*, 2021).

Assessing uncertainties in seismic tomography models is a challenge, because a formal resolution analysis is often not computationally feasible. In many cases, checkerboard tests are used with synthetic data that do not replicate the actual propagation paths nor are they faithful to the modal and frequency makeup of the observed waveforms. Lèvêque *et al.* (1993) showed that checkerboard tests can be misleading, and that, contrary to generally accepted ideas, smaller-size structures can be well retrieved, whereas larger-size structures for the same data coverage are poorly retrieved. However, this issue is often ignored, and more rigorous methods of quantifying model resolution are required.

Three key global-scale issues are the anisotropy, attenuation, and viscosity of the Earth’s mantle, and seismic tomography can make a major contribution in this area of research. Seismic anisotropy can be a key indicator of flow in the mantle. Models for 2Θ azimuthal anisotropy from Rayleigh waves are converging, but there are few 4Θ azimuthal anisotropy measurements from Love waves. Radial anisotropy could potentially help distinguish between horizontal and vertical flow in the mantle. However, existing models of radial anisotropy, when showing general agreement, on scales of

thousands of kilometers, display little agreement for smaller scale features. Extracting 4 Θ azimuthal anisotropy and radial anisotropy depends on the analysis of horizontal-component data, which almost always contains higher noise than vertical-component data. Some studies have exaggerated the radial anisotropy problem using Love- and Rayleigh-wave results from different sources, causing nonuniform path coverage. In addition, where radial anisotropic models are derived purely from fundamental mode data, additional issues arise because, for a given period, Rayleigh and Love waves sample the subsurface differently.

S-wavespeed models for the mantle show good agreement, but mantle attenuation models differ significantly in terms of both the geometry and magnitude of the variations. Such problems are not surprising, because it is more difficult to measure variations in the amplitude of a seismic wave than it is to determine its arrival time. It is not even straightforward to calculate the amplitude variations for a particular model, because lateral velocity variations lead to amplitude variations due to focusing and defocusing. Despite such problems, all authors who have studied mantle attenuation have remarked that attenuation and shear wavespeed are generally correlated.

Estimates of the 3D thermal structure of the upper mantle have been deduced from seismic tomography (e.g., [McKenzie et al., 2005](#); [Priestley and McKenzie, 2006](#); [Cammarano et al., 2011](#); [Priestley and McKenzie, 2013](#)) and so achieved reasonable resolution. However, 3D viscosity structure remains poorly resolved, despite being an important factor in mantle convection patterns (e.g., [Bunge and Richards, 1996](#)) and in controls on the evolution of sea level. The recent observations from Antarctica, where strong upper mantle contrasts in viscosity likely exist, show that ignoring 3D variations in viscosity can lead to significant errors in understanding the Global Positioning System uplift rate, water/ice mass balance, and sensitivity to changes in ice thickness (e.g., [van der Wal et al., 2015](#); [Powell et al., 2020](#)). Therefore, many applications that require a 3D viscosity model have derived it from seismic tomographic images (e.g., [Lau et al., 2018](#)). Such conversions are largely based on empirical choices of scaling relationships between seismic wavespeed and viscosity (e.g., [Austermann et al., 2013](#)), but the recent work has combined seismic tomography results with laboratory results to derive a “less” ad hoc relationship between seismic wavespeed and viscosity (e.g., [Priestley and McKenzie, 2013](#); [Priestley et al., 2024](#)).

MULTIPARAMETER INVERSION: ALL OR NOTHING!? (Andreas Fichtner)

Tomographic inversions for isotropic P and S wavespeeds have long been a standard, because reliably measurable body-wave arrival times and surface-wave dispersion are primarily sensitive to these parameters. Parameters with mostly smaller sensitivity, including anisotropy, attenuation, and density, continue to be comparatively weakly constrained, despite their

fundamental role in studies of temperature, composition, and flow inside the Earth. Although it would be desirable to constrain these parameters all at once, practical inversions limit the number of parameters to not more than a handful. In addition to computational cost, the fundamental reasons are (1) the increasing impact of subjective regularization choices as sensitivity decreases, and (2) our inability to independently constrain a large number of parameters with the available data.

The difficulty of multiparameter inversion can be explained mathematically with the help of Newton’s method (e.g., [Kennett and Sambridge, 1998](#)). Though not often used in practice, it allows us, in principle, to constrain a vector \mathbf{m} with components m_i representing the distributions of wavespeeds up to 21 elastic tensor components, attenuation, and so forth. Denoting by \mathbf{g} and \mathbf{H} the gradient and the Hessian of the misfit functional χ , Newton’s method yields the model update $\delta\mathbf{m} = -\mathbf{H}^{-1}\mathbf{g}$. If all parameters were uncorrelated, the resulting diagonal Hessian would allow us to consider each parameter individually via $\delta m_i = H_{ii}^{-1}g_i$. Any parameter m_i could either be included or dropped at will without affecting inferences of other parameters $m_{j \neq i}$. In reality, parameters are correlated, and the update is given by the following equation:

$$\delta m_i = H_{ii}^{-1}g_i + \sum_{n \neq i} H_{in}^{-1}g_n. \quad (1)$$

Other optimization algorithms and quasi-Newton methods, in particular, effectively produce equation (1) through iterative updating ([Nocedal and Wright, 1999](#)). Equation (1) contains an obvious contradiction to item (2) above. When significant trade-offs between parameters, described by the off-diagonal elements of \mathbf{H}^{-1} , are expected, these parameters can actually not be dropped. However, when trade-offs are small, the corresponding parameters may just as well be included. Furthermore, equation (1) demonstrates that, in contrast to common practice, the choice to include a parameter m_i cannot be based solely on the size of its sensitivity g_i . Instead, knowledge about the cumulative trade-offs with all other parameters, $\sum_{n \neq i} H_{in}^{-1}g_n$, is required. In this sense, we may be in the fortunate situation that a parameter with small sensitivity is comparatively well constrained, because the cumulative trade-offs with other parameters are small. Conversely, a parameter with large sensitivity may be difficult to resolve when trade-offs with seemingly unimportant parameters have a large cumulative effect.

Although second-order adjoint techniques ([Santosa and Symes, 1988](#); [Fichtner and Trampert, 2011](#)) provide efficient access to individual Hessian-vector products, the computation of $\sum_{n \neq i} H_{in}^{-1}g_n$ for a large number of parameters is computationally demanding. Therefore, we lack an easy criterion to inform us about the parameters that should be included or may be dropped.

The most profound consequence is that we cannot proceed incrementally, because we do not know which the next

meaningful increment should be. Including some of many parameters that describe anisotropy may be as (un)justified as including a parameter for attenuation, because the cumulative trade-offs with all other parameters are unknown. Experimental design approaches either at the level of model parameters (Sieminski *et al.*, 2009) or misfit functionals (Bernauer *et al.*, 2014) may help suppress parts of $\sum_{n \neq i} H_{in}^{-1} g_n$ but still require information on \mathbf{H}^{-1} to check if this goal has actually been achieved. In the absence of a quantitative ordering, we may be forced to include all parameters to avoid artifacts caused by insufficiently informed decisions concerning their relative importance. This closes the circle to the regularization and trade-off problems (1) and (2), explained earlier.

Both problems can, in principle, be avoided by regularization-free Bayesian inference methods. Practical implementations of Bayesian inference, for instance, in the form of Hamiltonian Monte Carlo (HMC; Fichtner *et al.*, 2019) or variational inference (Zhang *et al.*, 2022) allow us to not only consider higher dimensional model spaces relevant for seismic tomography but also will require further improvements to solve large multiparameter problems. The design of meaningful priors that go beyond the standard Gaussian or constant distributions through the incorporation of petrological and geostatistical information will be instrumental in making multiparameter Bayesian inference efficient and practical.

UNCERTAINTY IN SEISMIC TOMOGRAPHY (Nicholas Rawlinson)

When presented with a “final model” produced by seismic tomography, which might contain coherent anomalies that appear ripe for interpretation, the first question one should always ask is “what can I believe”? This is an excellent question, because the inverse problem that lies at the heart of seismic tomography is ill-posed, with multiple models capable of satisfying the data. Of course, you might be tempted to say “wait; if I parameterize my model with one single constant velocity block, then the solution must be unique!” This fails on two levels: first, you have arbitrarily selected your parameterization, and an infinite variety of other options also exist that are equally (or probably more!) justifiable; second, you are unlikely to fit the data with a single parameter, and, even if you can, the presence of data noise precludes there being a unique solution. As noted by Keiiti Aki in his seminal article (Aki *et al.*, 1977), the ideal parameterization might ostensibly be one that has a scale length on par with the seismic wavelength. However, the data coverage will almost never be sufficient to make this a worthwhile endeavor. Irregular parameterizations where one attempts to vary the spatial scale length of the underlying parameterization (e.g., by employing an unstructured mesh) to somehow match the data coverage is a balancing act of trying to make the inverse problem as well posed as possible, while at the same time maximizing the extraction of information from the dataset (Bijwaard *et al.*, 1998; Fang *et al.*, 2019).

In addition to data noise and parametrization choice, there are other factors that contribute to model uncertainty. Typically one makes assumptions about anisotropy, since inverting for all 21 independent elastic moduli is generally out of the question; as a result, unmodeled anisotropy will manifest as model uncertainty in a way that is difficult to quantify. Assumptions in solving the forward problem will also play a role in model uncertainty, for instance, the use of ray theory to predict travel times is a well-known approximation that gets poorer as the ratio between seismic wavelength and structural wavelength increases. Unsurprisingly, the above issues are well recognized by the seismology community, and they have not been idle in seeking out novel approaches for addressing such challenges.

With ongoing increases in computing power, inversion methods that produce an ensemble of data-satisfying models rather than a single model are becoming more popular (Fichtner *et al.*, 2019; Zhang and Curtis, 2020). The advantage of this approach is that the ensemble can be interrogated for common features that are required by the data. An approach known as transdimensional (transD) tomography (Bodin and Sambridge, 2009; Bodin *et al.*, 2012), which employs a reversible jump Markov chain Monte Carlo (rj-McMC) scheme to construct a posterior probability density function (PDF) from a prior PDF and likelihood function within a Bayesian framework, has become quite popular in the recent years. It allows for the number of unknowns in the inverse problem to also be an unknown and through a hierarchical approach can include noise parameters in the inversion. Typical models are built on unstructured or nested parametrizations that are amenable to redistribution, densification, and removal in an effort to extract the maximum information from the data with the fewest parameters. The posterior PDF is typically distilled by taking the mean (or median) model as the “final” model and the standard deviation as a measure of uncertainty. This approach is less valid if the posterior PDF does not have a unimodal distribution. Despite the data driven nature of transD, like other tomography methods, it still depends on the quality of prior model information and data uncertainty estimates, which are often poor. As a consequence, it is not immune from the need to make ad hoc decisions to produce what can be regarded as “reasonable” results.

Because new methods continue to be developed and computing power increases, our ability to account for nonuniqueness of solution in seismic tomography will continue to improve. Perhaps the most challenging issue to deal with is data noise, since invariably it is poorly constrained, and even the distribution is generally not well understood. Most misfit or objective functions employ an L_2 measure of misfit, which is optimal if the noise has a Gaussian distribution, but otherwise is not robust to outliers, something that is difficult to guard against without removing potentially important data. Aside from methodological improvements, the use of increasingly

large volumes of data that include considerable redundancy is another important way forward. This can be seen in regional or global travel-time tomography, for example, where individual measurements may carry substantial picking error, but huge numbers of nearby earthquakes can be exploited to clean up signal (e.g., by clustering and stacking), which is essential for producing good models (Zenonos *et al.*, 2019). In exploration, the excellent coverage of (usually) high-quality data with inherent redundancy, coupled with good prior information, is largely responsible for the active-source version of full-waveform inversion (FWI) becoming a standard technique that can retrieve remarkably detailed and well-constrained images of the subsurface (Mancini *et al.*, 2016).

RESOLUTION OF (AN)ELASTIC MANTLE MODELS (Ebru Bozdağ)

Efficient numerical wave propagation solvers and high-performance computing (HPC) have opened new frontiers in passive-source seismic tomography by taking the full complexity of wave propagation into account in the inverse problem (e.g., Fichtner *et al.*, 2009; Tape *et al.*, 2009; French and Romanowicz, 2015; Bozdağ *et al.*, 2016; Lei *et al.*, 2020). Yet, it is challenging to “peel off” the outer heterogeneous layers of the Earth to image the target depths of interest where the complex physics of the medium and the seismic source must similarly be addressed in inversions. The ideal is to update all seismic parameters simultaneously (i.e., wavespeeds, density, anisotropy, anelasticity, and source parameters). However, the trade-off between parameters exacerbated by the uneven distribution of seismic sources and receivers concentrated at the surface makes such comprehensive inversion challenging.

Although full waveforms are computed numerically, the first-generation adjoint tomography models in earthquake seismology were built using phase measurements only. This choice was made to minimize the trade-off between model parameters by targeting the elastic properties of the media. Amplitudes of seismic phases are sensitive to the nonlinear combination of scattering/defocusing, anelasticity, source radiation pattern, and scalar moment (e.g., Dalton *et al.*, 2008). Yet, if they can be assimilated properly, amplitudes can provide unique constraints to locate heterogeneities (e.g., Laske and Masters, 1996), because they are sensitive to the gradient of phase speeds (Woodhouse and Wong, 1986). However, one needs to address the anelasticity and source parameters with the elastic structure, specifically at the global scale.

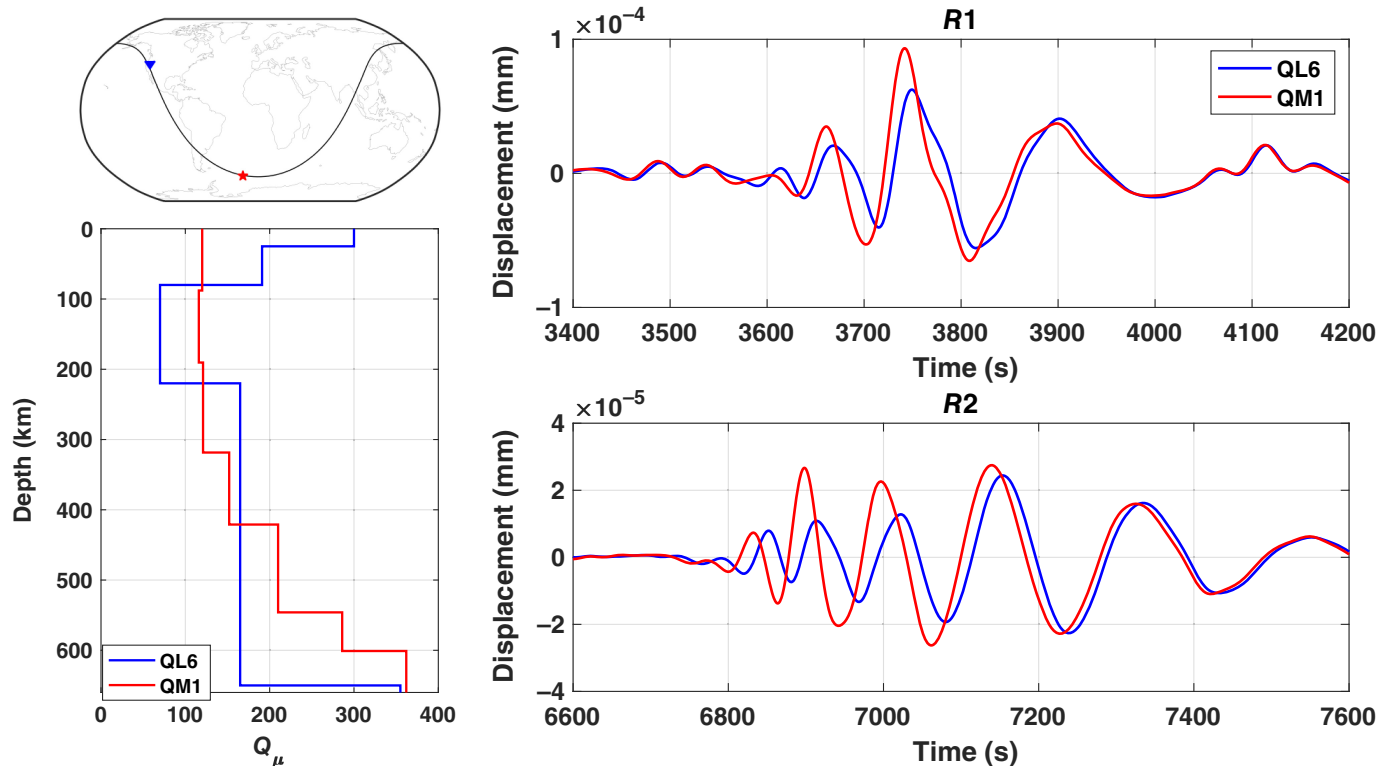
Attenuation (Q^{-1} , inverse of quality factor Q) models are important not only for constraining the water content, partial melting, and temperature variations in the mantle (e.g., Anderson, 1967; Karato and Jung, 1998) but also for the character of elastic models. It is generally assumed that a suitable radially symmetric Q^{-1} model can capture the physical dispersion of seismic waves (e.g., Kanamori and Anderson, 1977). However, there is no consensus even on the 1D Q

structure (e.g., Resovsky and Trampert, 2002). This leads to two major consequences for elastic models:

1. Wavespeeds of elastic models involve physical dispersion from the Q^{-1} models used in their inversion, which is often significant and needs to be corrected before any model comparisons.
2. Because elastic models are constructed as perturbations around chosen Q^{-1} models, any uncertainty in Q^{-1} may be mapped onto elastic models.

Figure 3 shows a simple comparison of minor-arc and major-arc Rayleigh waveforms computed for the same elastic model—GLAD-M25 (Lei *et al.*, 2020)—but with different Q^{-1} models in the upper mantle: QL6 of Durek and Ekström (1996) and QM1 of Widmer *et al.* (1991). The waveforms are filtered between 40 and 250 s—a typical period band for surface-wave data in global tomographic studies. For this example, Q^{-1} models cause ~ 22 s time shift on the major-arc Rayleigh wave, which is more than half a cycle of the minimum period of the waveforms. The effect of the different Q^{-1} models is less on body waves but still can be significant relative to their measured time shifts. Therefore, it is essential to perform FWIs by simultaneously updating Q^{-1} and elastic models not only to construct Q^{-1} models to provide additional constraints on the mantle’s thermochemical structure but also to continue to improve the elastic models.

However, in practice, it is challenging, if not impossible, to independently retrieve elastic and anelastic models due to uncertainties in the nature of the medium (i.e., anisotropy) and source parameters. One recommended approach is the sequential inversion of elastic and anelastic parameters, which allows mitigation of the trade-off at each iteration (e.g., Karaoğlu and Romanowicz, 2018). Designing appropriate measurements to be used for FWIs, such as those based on amplitude ratios of different phases (e.g., Ritsema *et al.*, 2002) or double-difference phase misfits (Yuan *et al.*, 2016), may help reduce source uncertainties. Still, the problem of fully characterizing the anelastic Earth is complex due to the trade-offs between seismic parameters, and better resolution can only be achieved by updating elastic and anelastic parameters simultaneously or sequentially. This issue highlights the importance of uncertainty quantification in tomographic models. Meanwhile, the problem of adequate resolution is naturally worsened by the uneven global data coverage where we need more data, specifically from oceans. Emerging technologies such as distributed acoustic sensing, nodal arrays, and so forth provide unprecedented sampling of the continents and offshore, complementing dense broadband arrays. MERMAIDs (e.g., Simons *et al.*, 2021) are promising to efficiently sample the oceans by acoustic means, while we ultimately would like to see USArray-type ocean-bottom seismometer arrays. All these new opportunities need to be carefully analyzed and integrated



into seismic tomography to maximize the benefits of emerging instruments and big data in seismology.

WHAT ARE TOMOGRAPHY'S LIMITATIONS? (Jeroen Ritsema)

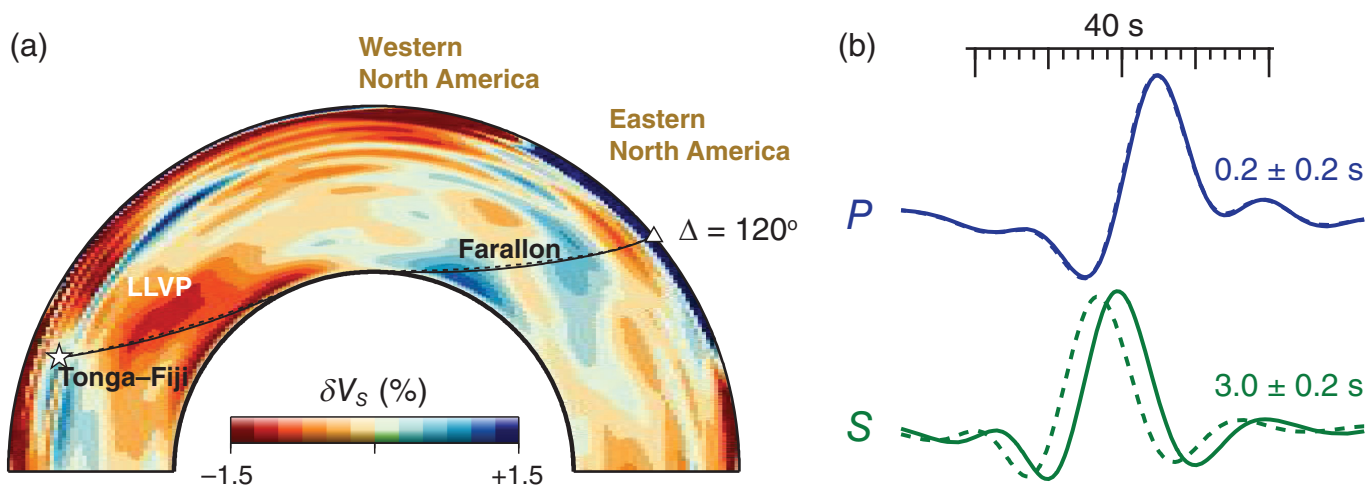
For many end users, tomography is a black box that magically turns seismic data into tantalizing pictures of Earth's interior. Convenient tools like SubMachine (Hosseini *et al.*, 2018) help scientists explore the images and reconcile velocity anomalies with other geophysical observations. It is fair for seismologists to present tomography as an important technique for mapping Earth's composition, but they must expose tomography's observational constraints, modeling choices, and other secrets. Image resolution is heterogeneous and uncertainties are uncertain, no matter which tomographic model is one's favorite.

Even the biggest structures in tomographic maps are not fully understood. A case in point is the nature of the large, low-velocity provinces (LLVPs) that may play a key role in global mantle circulation (e.g., McNamara, 2019). "Vote maps" of V_S models agree on the LLVPs' areal extent (Cottaar and Lekic, 2016), but mineral physicists want V_S and V_P and geodynamicists want density. The V_P structure at the core–mantle boundary is poorly resolved, because diffracted P waves have a short reach, PcP signals are weak, and no seismometer on Earth has recorded a PKP wave through LLVPs. The travel times of P waves from earthquakes in the Tonga region to seismometers in North America form the bulk of the P wave constraints on the Pacific LLVP. In eastern North America, these P waves are recorded with a delay of less than 1 s, whereas the average S -wave delay is 5 s.

Figure 3. Effect of upper-mantle attenuation on vertical-component minor-arc and major-arc Rayleigh waves (right panel) where the corresponding ray paths are shown top left. Simulations are performed for the 3D mantle model GLAD-M25 (Lei *et al.*, 2020) with 1D Q model QL6 (Durek and Ekström, 1996) (blue) and with QM1 (Widmer *et al.*, 1991) in the upper mantle (red), as shown bottom left. Seismograms were computed by the 3D global wave propagation solver SPECFEM3D_GLOBE (Komatitsch and Tromp, 2002) and filtered between 40 and 250 s. Figure courtesy by Ridvan Örsüran. The color version of this figure is available only in the electronic edition.

"Reasonable" estimates of the V_S and V_P structure can explain these travel-times delays (Fig. 4), but the $\ln V_S / \ln V_P$ ratio of the LLVP, important for differentiating thermal and chemical origins of seismic heterogeneity (e.g., Karato and Karki, 2001), depends on the resolution of V_P of the North American lithosphere. Constraints on the LLVP's density depend on V_P and other factors (Robson *et al.*, 2022). It remains uncertain whether LLVPs are relatively dense or light.

It is natural that tomography takes advantage of super computers and "big data" approaches. The use of fuller waveforms with higher-frequency content will enhance image resolution on global (e.g., French and Romanowicz, 2014; Lei *et al.*, 2020), regional (e.g., Cupillard *et al.*, 2012), local (e.g., Tape *et al.*, 2010), and multiscales (e.g., Fichtner *et al.*, 2018). Deployments in the oceans (e.g., Suetsugu and Shiobara, 2014; Tsekhmistrenko *et al.*, 2021; Pipatprathanporn and Simons, 2022) and in countries such as China (Yuan and Xu, 2019), Brazil (Bianchi *et al.*, 2018), and on the African continent (Nyblade *et al.*, 2011), where



global network coverage is relatively low, are essential to diversify wave coverage. New techniques for the modeling of body-wave triplications (Stahler *et al.*, 2012), and wave conversions (de Jong *et al.*, 2022) and reflections (Guo and Zhou, 2019) at the “410” and “660” km discontinuities may help improve the relatively poor resolution in the transition zone—a layer known to impede convective flow.

It is also important to collaborate with the users of tomography to ensure that our geophysical research questions are in sync and to optimize tomography as the best tool for the testing of hypotheses of deep-Earth physics. Image visualization must be accompanied with practical tools for interrogating image resolution. Mapping Earth’s structure with finer detail remains a worthwhile effort, but *how does Earth work* is not a question for tomographers alone.

PRESENTATION AND COMPARISON OF TOMOGRAPHIC MODELS (Brian L. N. Kennett)

Many decisions have to be made in setting up a tomographic model, and some, such as the choice of the position of discontinuities, can have significant effect on the actual outcome. Such effects are noticeable in global models because of the influence of the major discontinuities in the mantle transition zone. There is a tendency for apparent heterogeneity to increase in the neighbourhood of assumed discontinuities, which may be real but can arise from misplacement of interfaces. The presence of strong discontinuities in the base model employed without direct correspondence in the data can lead to notable distortions in the extracted results. For example, the very strong 210 km discontinuity in preliminary reference Earth model (PREM; Dziewoński and Anderson, 1981) produces distinctive effects in inversions that are not present when no discontinuity is introduced (Kustowski *et al.*, 2008).

Another class of prior assumptions that can have significant effects on the outcome relate to the continuity of heterogeneity structure. In global models, a common choice is to allow different styles of behavior above and below the “660 km”

Figure 4. (a) The degree-12 V_S structure S12—similar to other global-scale tomographic V_S models for the mantle (e.g., Ritsema and Lekić, 2020)—along a great circle through the southwestern Pacific region on the left and North America on the right. The star indicates the hypocenter of an earthquake beneath Tonga–Fiji. The triangle is at an epicentral distance of 120° . (b) Spectral element method (Komatitsch and Tromp, 1999) waveforms of the P and SH wave for a distance of 120° , computed for (dashed lines) preliminary reference Earth model (PREM; Dziewoński and Anderson, 1981) and (solid lines) S12 and P12. P12 differs from S12 by a scaling factor R that increases from 1 in the upper mantle to 3 in the lower mantle, consistent with global travel-time measurements (e.g., Robertson and Woodhouse, 1996; Ritsema and van Heijst, 2002). The numbers on the right indicate the misalignment between the S12/P12 and PREM signals. The P wave’s deceleration in the large low-velocity provinces (LLVP) and its acceleration in the Farallon anomaly and the lithosphere of eastern North America are equal, so the P -wave arrival time is the same as the PREM predicted arrival time. This figure is a modification of figure 9 in Chaves *et al.* (2020). The color version of this figure is available only in the electronic edition.

discontinuity to separate upper and lower mantle, as, for example, in the model GLADM-25 (Lei *et al.*, 2020) obtained with FWI. However, the mantle transition zone extends further in depth with garnet phases only eliminated at about 800 km; so this choice is more arbitrary than it seems. There is a strong evidence for significant viscosity contrast between the uppermost mantle and the deeper parts, but the depth of the end of the viscosity increase is not well constrained. Placing a discrete boundary for heterogeneity coincident with the wavespeed jump is a specific assumption.

Because knowledge of 3D structures has grown, it is less common for tomographic results to be obtained by a single-pass linearized inversion from a reference model. But still most models are created and stored as a set of perturbations from some reference. In the case of inversions based purely on relative travel times it is not entirely clear what this reference may be. Where possible, the inclusion of absolute timing can help resolve such issues. Intercomparison of 3D models is facilitated by presenting results in terms of absolute velocities. This approach also has the merit that any impact from an underlying reference model is fully represented.

Many tomographic results are plotted as perturbations from radial reference models that have been chosen for convenience or constructed in association with the 3D model, such as model GAP_P4 (Obayashi *et al.*, 2013), and the radial profile for GLADM-25 (Lei *et al.*, 2020). Such a procedure may appear a natural consequence of model construction but can obscure the impact of specific assumptions or features in the underlying model. Authors should be encouraged to present their plots relative to well-known reference models. Suitable comparator models should have relatively bland properties with the minimal presence of discontinuities. In this way direct visual and numerical comparison between different styles of models is facilitated. STW105 (Kustowski *et al.*, 2008) is a good choice as a reference for long-period work, because it retains the lower mantle character of PREM without as much shallow complexity. For higher frequency work, ak135 (Kennett *et al.*, 1995) has proved quite effective for a wide range of both *P* and *S* studies.

It is important to exploit the full available control on the physical properties of the Earth, especially where comparisons are to be made with mineral physics predictions. In this context comparison of wavespeed models from different wavetypes with differing resolution can lead to potentially misleading conclusions. For the full mantle, *S* coverage is more readily secured than for *P*, but in regional studies *P* readings are likely to be much more plentiful than for *S*, as in the work of Zhao *et al.* (2021).

For travel-time tomography comparable coverage can be achieved by choice of only paths for which both *P* and *S* have been picked (Kennett *et al.*, 1998; Gorbатов and Kennett, 2003). This approach not only provides a quality control filter on the data but also means that wavespeed ratios are meaningful. In these circumstances it is useful to look at joint tomography to extract bulk-sound speed as well as *P* and *S* properties (Kennett *et al.*, 1998). For FWI, good *P*-wave coverage to supplement *S* can be achieved if appropriate windows of seismograms are exploited, though the generally smaller amplitudes of *P* phases can mean reduced sensitivity.

Ideally comparisons of images for different wavetypes should be made with comparable wavelength for *P* and *S* sampling. Except in areas of high attenuation, the frequencies of *S* arrivals for teleseisms are roughly half those for *P*. Thus, *P* and *S* wavelengths are similar. For waveform inversion, the maximum frequency employed is likely to be dictated by computational considerations, but selective filtering can help with equalization.

FWI FOR GLOBAL MANTLE STRUCTURE, WHAT'S NEXT: (Barbara Romanowicz)

A fundamental requirement for successful tomographic imaging is the appropriate illumination of the target region requiring each subvolume to be sampled by waves propagating in different directions. This requirement is even more severe when the structure sampled is seismically anisotropic. As well-meaning

mathematicians have shown (e.g., Castelvocchi, 2017), if the Earth's surface were densely and uniformly covered by both sources and receivers, we could uniquely resolve the seismic structure of the mantle, at least its isotropic part, using only *P* and *S* travel times. In practice, such a proposition is unrealistic. So, more information needs to be extracted from each seismogram to compensate for the uneven and often sparse distribution of earthquake sources and stations. This is where the power of FWI lies; it makes it possible to exploit the information contained in every wiggle of a seismogram, produced by all the different seismic waves that bounce and scatter inside the Earth, whether or not they can be easily separated on the record.

FWI requires the computation of the complete seismic wavefield in a 3D Earth. Although early global FWI models were based on normal-mode perturbation theory (Woodhouse and Dziewoński, 1984; Li and Romanowicz, 1996; Mégnin and Romanowicz, 2000), a major step forward was the introduction to global seismology of an efficient method to solve the wave equation numerically—the spectral-element method (SEM; Komatitsch and Vilotte, 1998; Komatitsch and Tromp, 1999), which lifted restrictions on the smoothness and wavelength of the 3D structure at the expense of increasing computation time, which grows as the fourth power of frequency. Importantly, it made it possible to compute accurate misfit surfaces. This led to first generation global mantle models that compute the forward wavefield accurately using SEM (Lekić and Romanowicz, 2011; French and Romanowicz, 2014; Bozdağ *et al.*, 2016; Lei *et al.*, 2020) but differ in their inversion methodologies, and, in particular, in the way sensitivity kernels are computed. A comparison and discussion of the pros and cons of the different choices made for data processing and inversion used in these two approaches is presented in Romanowicz (2023).

In addition to exploiting the main phases bouncing between the surface and the core–mantle boundary, FWI based on the SEM (or other accurate numerical methods for wavefield computation) has the potential of exploiting information in the coda of the main seismic phases, which is particularly important for resolving low-velocity regions of small dimensions hidden from view in conventional travel-time measurements by the phenomenon of wavefront healing (e.g., Nolet and Dahlen, 2000). This is already apparent in the emerging resolution of deep mantle plumes in the latest SEM-based models (e.g., French and Romanowicz, 2015; Lei *et al.*, 2020).

Going forward, one possible way to improve resolution in FWI is to work toward reaching higher frequencies, which comes at great computational expense. However, illumination becomes a problem again. Although it is essential to keep maintaining the high-quality international global very broadband seismic network and complementing it by regional, continental, and especially seafloor deployments, including efforts such as MERMAIDS (Sukhovich *et al.*, 2015); achieving high resolution uniformly at the global scale is not a realistic goal. Promising approaches are using adaptive grids that can be

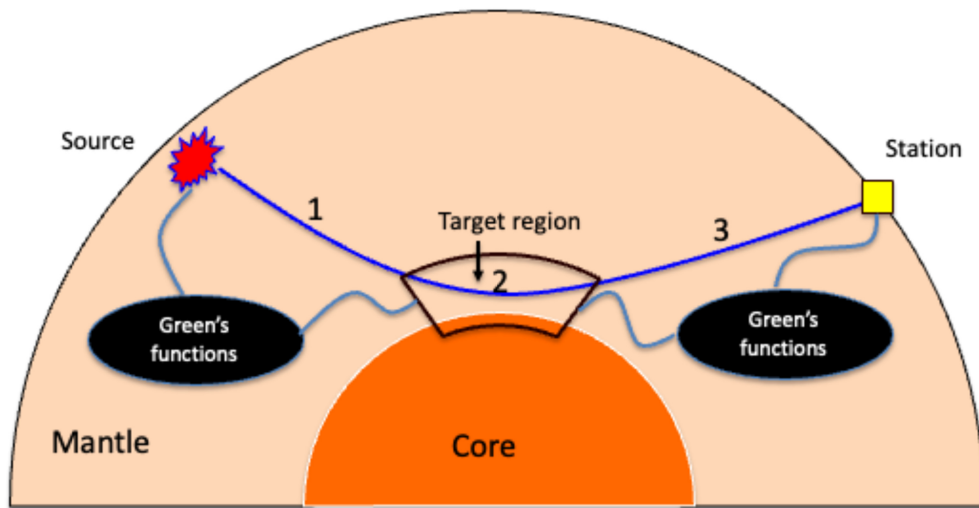


Figure 5. Box tomography is set up for imaging of a remote target region in the Earth. The Green's functions (1) and (3) are precomputed in a reference global model and recorded at the boundaries of the target region. Full-waveform inversion (FWI) proceeds with wavefield computations restricted to the target region (2). Time reversal mirrors allow the reconstruction of the full wavefield from the remote source to the remote station at each iteration. The color version of this figure is available only in the electronic edition.

refined in well-illuminated regions (e.g., Thrastarson *et al.*, 2020), or, alternatively, aiming to resolve well-illuminated regions of geophysical interest, possibly complemented by targeted, long duration, broadband instrument deployments. For targets in the deep mantle, farther away from sources and stations (for example roots of mantle plumes), such an approach would still require heavy computations if the entire wavefield is recomputed at each iteration. Here, a particularly promising methodology is “Box Tomography,” in which the wavefield computations are broken into three parts: (1) from the source to the boundary of the target region, (2) within the target region, and (3) from its boundary to the recording stations. The long-distance wavefields in (1) and (2) are computed only once in the best possible, relatively smooth, background model, whereas model iterations are performed only within the box (Fig. 5). This separation can significantly reduce computational time, and the illumination requirement needs only to be verified within the target region. Concerns have been raised about mapping unmodeled outside heterogeneity into the box. However, with robust illumination by crossing paths within the box, such outside structure affects only a specific swath of paths and will be incompatible with measurements on paths from other directions, which will prevent its projection into the box. Masson and Romanowicz (2017) illustrated the power of such an approach (albeit in 2D) by showing how the structure in a box located at the CMB can be recovered even if the background mantle model is assumed to be 1D. Such box methodology is under development using existing SEM-based computational tools (e.g., Leng *et al.*, 2020; Adourian *et al.*, 2021; Pienkowska *et al.*, 2021). In the future, it should be able

to take advantage of novel, more efficient solvers (e.g., Masson, 2023) and may eventually lend itself, within relatively small target regions, to full-waveform Bayesian inversion in 3D or other artificial intelligence methodologies.

ADJOINT WAVEFORM TOMOGRAPHY FOR NEXT-GENERATION SEISMIC ANALYSES AND MONITORING (Arthur J. Rodgers)

The development of methods and capabilities to compute complete waveform simulations in 3D Earth models along with adjoint methods for computing the fully 3D sensitivity kernels in the 2000s (e.g., Tromp *et al.*, 2005; Fichtner *et al.*,

2006) set the stage for new advances in seismic imaging (Tromp, 2020). In my opinion, the full benefits of adjoint waveform tomography (AWT) are not yet fully realized, and this will be an important direction for the future of seismic tomography.

FWI has the advantage of fitting the data we actually record on seismometers rather than derived observables, and perhaps more importantly it includes the full finite-frequency sensitivity to 3D structure. The framework of AWT includes the necessary physical material properties needed to simulate waveforms in 3D (i.e., shear and compressional wavespeeds, anisotropy, density, attenuation, and discontinuities), although not all may be solved for. However, FWI comes with challenges; most importantly, it is both data and computationally intensive. Large datasets (many events and receivers) are needed to provide azimuthally distributed and redundant geographic sampling to triangulate anomalies. Many iterations are needed to converge inversions of longer-to-shorter period waveforms through a conservative multiscale approach. The main challenges are the computational effort needed to compute forward and adjoint simulations for many events and many iterations, and the processing of all waveform windows and misfits. The recent advances in AWT workflow efficiency implemented in dedicated software packages such as the large-scale seismic inversion framework (LASIF; Krischer *et al.*, 2015; Thrastarson *et al.*, 2021), SeisFlows (Modrak *et al.*, 2018), Pyatoa (Chow *et al.*, 2020), or Salvus (Afanasiev *et al.*, 2019) and HPC platforms, for example, hybrid central and graphics computing unit acceleration, large shared memory nodes, are making it possible to run more iterations on larger datasets more quickly than was previously possible. It

is important not to forget that waveform inversion can also suffer from the problems that plague all seismic tomographic inversions (e.g., data coverage, uncertainties in source parameters, model parameterization, and regularization). However, the fully 3D sensitivity of the complete waveform to structure enables AWT to use scattered arrivals and constrain larger volumes of the Earth compared to traditional methods (e.g., ray theory, path-average approximation). [Rodgers et al. \(2022\)](#) ran a multiscale AWT inversion for the western United States and used about ten times more iterations compared to the previous studies. The resulting WUS256 model provided greatly improved waveform fits over the previous models based on AWT and surface-wave dispersion tomography.

The promise of AWT is to provide 3D models that can reliably simulate observed waveforms. The current research must focus on evaluation of the validity of 3D seismic models obtained with AWT, including investigations of how models perform for other seismic observables (e.g., body-wave travel times and surface-wave dispersion). This community must discover and understand the limitations of AWT to achieve good waveform fits at shorter periods resolving finer-scale structure. That is: What kinds of waveform data and measurements are needed to improve the coverage? How can validation and resolution be reliably assessed? How can computational resources be most efficiently used, especially as the effort of simulations increases as frequency to the fourth power?

The benefits of 3D Earth models fitting shorter periods are manifold not only for geologic/tectonic interpretation of structure but also for immediate societal applications such as seismic hazard and operational earthquake and explosion monitoring. One important target would be to image the upper crust in areas of high seismic risk on subkilometer scales for earthquake strong-motion simulation and analysis (frequencies of ~ 1 Hz or higher). Another use case would be regional-scale source characterization (location, depth, and moment tensor) with full waveforms for seismic hazard, reservoir, and mine seismicity as well as sparse network global explosion monitoring (e.g., the Comprehensive Nuclear-Test-Ban Treaty International Monitoring System).

If AWT models prove successful at reproducing independent waveform observations, they will be useful for these and other analyses. Green's functions for proven models could be precomputed on HPC using reciprocity for a fixed network of stations and made available via web or cloud services. Although the storage requirements for regional-scale Green's function databases are tremendous, this would make synthetic seismograms for 3D models available for immediate (e.g., operational pipeline) use without the need to run arduous event-specific HPC simulations. Furthermore, such stored seismograms enable probabilistic (stochastic) forward and inverse calculations of ground-motion intensity or source properties. The benefits and use cases for improved waveform-based 3D seismic Earth models await for the seismic tomography

community to fully realize the advances that were previewed in Toronto and are highlighted in this special issue.

ADVANCING WAVEFORM INVERSION BASED ON SOURCE ENCODING AND MODEL-ORDER REDUCTION (Jeroen Tromp)

Thanks to modern numerical methods and high-performance computers, seismic FWI has been fully realized, as envisioned by [Bamberger et al. \(1977\)](#), [Lailly \(1983\)](#), and [Tarantola \(1984\)](#). FWI is now used across nine orders of frequency and wavelength, from megahertz frequencies and millimeter wavelengths in ultrasound medical imaging and nondestructive testing to millihertz frequencies and thousand-kilometer wavelengths in earthquake seismology. The ultimate goal of FWI is to use every wiggle in a seismogram to understand the Earth's physics and chemistry.

FWI is continually being developed and improved, with the potential for a more complete description of the physics of seismic wave propagation and better optimization algorithms. Numerous reviews, such as those by [Virieux and Operto \(2009\)](#), [Fichtner \(2010\)](#), [Liu and Gu \(2012\)](#), and [Tromp \(2020\)](#), provide further insight into the advancements of FWI.

In this section, I will provide a brief overview of three promising methods: source encoding, model-order reduction, and HMC. Combining model-order reduction with source encoding can lead to a significant shift from using iterative quasi-Newton local optimization methods to HMC global optimization methods. This shift enables faster and high-resolution imaging, while also allowing for uncertainty quantification. Speed is crucial for time-sensitive imaging, such as mammography. In addition, the interpretation of FWI tomographic images requires accurate quantification of uncertainties to assess the thermochemical origin of wavespeed variations in the Earth's deep interior.

Source encoding

In traditional time-domain FWI, an inversion is independent of the number of receivers but scales linearly with the number of sources. To ameliorate this problem, exploration seismologists developed source encoding ([Ben-Hadj-Ali et al., 2009](#); [Krebs et al., 2009](#); [Choi and Alkhalifah, 2011](#); [Schuster et al., 2011](#); [Schiemenz and Igel, 2013](#); [Castellanos et al., 2015](#); [Zhao et al., 2016](#)), in which data from different sources are combined in one encoded "supergather." The challenge had been that the encoded contributions from distinct sources are difficult to completely unravel, leading to "crosstalk" ([Romero et al., 2000](#)), which contaminates Fréchet derivatives. Recently, successful methods of crosstalk-free source encoding have been developed ([Huang and Schuster, 2012, 2017](#); [Krebs et al., 2013](#); [Zhang et al., 2018](#); [Tromp and Bachmann, 2019](#); [Bachmann and Tromp, 2020](#)). In the approach of [Zhang et al. \(2018\)](#) and [Tromp and Bachmann \(2019\)](#), encoded forward and adjoint wavefields are run until they reach a steady state, at which point they are "decoded" based on integration over a time interval that is the

reciprocal of the encoded frequency spacing to obtain their stationary parts. These parts are combined for all sources to obtain crosstalk-free Fréchet derivatives.

The main drawback of crosstalk-free source-encoded formulations arises from the difficulty of time windowing modeled data when inverting one or a few sparsely sampled frequencies at a time and so selecting specific arrivals for the various stages of the inversion. To overcome this limitation, [Cui et al. \(2023\)](#) and [Liu et al. \(2024\)](#) propose the use of complex-valued frequencies through the Laplace transform, which damps arrivals at a certain rate starting from a given travel time. This approach focuses the inversion on first-arriving body waves and suppresses difficult-to-fit surface waves. Because the iterations progress, the damping is gradually reduced, thereby blending in the later arrivals.

Model-order reduction

In model-order reduction ([Rozza et al., 2008](#); [Quarteroni et al., 2016](#)), the system of equations for FWI is projected onto a lower dimensional space to reduce computational and memory requirements at the cost of introducing approximation errors. [Hawkins et al. \(2023\)](#) have recently demonstrated that model-order reduction shares similarities with classical normal-mode theory ([Dahlen and Tromp, 1998](#)). More generally, [Hawkins et al. \(2023\)](#) demonstrate how model-order reduction can be used for rapid calculations of seismograms in inverse problems, creating new opportunities for time-critical FWI applications.

HMC sampling

The HMC method ([Duane et al., 1987](#)) is a Markov Chain Monte Carlo (MCMC) technique that uses derivatives of the PDF to efficiently sample the posterior distribution ([Neal, 2011](#); [Betancourt, 2017](#)). Thus, whereas MCMC requires just evaluations of the misfit, HMC also requires the misfit gradient, which may be accomplished based on the adjoint-state method used in traditional FWI. There are promising first applications of HMC techniques for tomography ([Fichtner et al., 2019](#)) and uncertainty quantification ([Fichtner and Zunino, 2019](#)).

In summary, I foresee many future opportunities for FWI across scales, for example, based on ultrasound for medical imaging and nondestructive testing or to probe the Earth's critical zone ([Eppinger et al., 2024](#)). In all such applications, crosstalk-free source encoding and model-order reduction methods could be game changers, especially when combined with Bayesian inference accelerated by HMC techniques. Machine learning and data analytics are likely to significantly impact FWI, especially in the contexts of data assimilation and feature extraction.

FWI APPLICATION TO TELESEISMIC WAVES BENEATH DENSE ARRAYS (Qinya Liu)

The past two decades have witnessed growing applications of FWI techniques that generate high-resolution and high-fidelity

images at both global and regional scales (see [Tromp, 2020](#) for a review). Most tectonic-scale FWI studies have relied on local earthquake data. But for seismic array deployments, FWI can also take advantage of other standard datasets used in seismic array analysis, particularly for regions with limited local seismicity. One such dataset is converted/scattered waves of teleseismic phases (referred to as teleseismic waves hereafter). Significant progress has been made in the past decade to apply FWI to teleseismic waves on dense arrays (TeleFWI). This approach is different from ray-based receiver function (RF) and inverse scattering approaches. To avoid the exorbitant numerical cost of full global simulation at teleseismic distances, TeleFWI uses hybrid methods to simulate the propagation of teleseismic waves (e.g., *P*) into a confined domain beneath an array (e.g., [Monteiller et al., 2013](#); [Tong et al., 2014](#)) by interfacing 1D solvers with regional 3D solvers and can model high-frequency scattered waves down to $\sim 1\text{--}3$ s. The adjoint simulation and inversion iterations can be then carried out similarly as standard FWI practices.

TeleFWI has enabled some impressive fine-scale lithospheric imaging beneath dense array in the recent years (e.g., [Wang et al., 2016](#); [Beller et al., 2018](#); [Kan et al., 2023](#)). However, it remains both encouraging and challenging in several aspects.

Datasets

Lithospheric imaging based on TeleFWI generally requires the station spacing to be $<10\text{--}15$ km to avoid spatial aliasing, which largely restricts it to dense linear array deployments instead of regional 2D areal networks. On the other hand, as most temporary dense array deployments are just for 1–3 yr, the requirement of coherent and slowly varying teleseismic waveforms across an array often severely limits the number of events (typically <0) and the period band (typically ≥ 5 s) used in TeleFWI compared to tens to hundreds of events available for RF analysis and inverse scattering. Nevertheless, TeleFWI studies have successfully imaged lithospheric targets with only a handful of events, sometimes as few as five ([Wang et al., 2016](#)). With the recent theoretical development of finite-frequency kernels for receiver functions ([de Jong et al., 2022](#)), efforts have been made to use the deconvolved RFs themselves ([Xu et al., 2023](#)) which eliminates the need for source time function estimation, improves the signal-to-noise ratio (SNR) of the inverted data, and pushes the inverted period band down to 1–3 s. In addition to teleseismic *SH* waves ([Kan et al., 2023](#)), another dataset to explore is teleseismic *SV* scattered/converted waves used in *S* RFs. However, their limited epicentral distance range and lower SNR may result in even fewer usable events, and therefore may only work when combined with other datasets.

Robustness tests

Synthetic studies need to be conducted to further understand the robustness of TeleFWI or RF-based TeleFWI, such as the

impact of initial models (Beller *et al.*, 2018) and the presence of shallow/slow sedimentary basins. In particular, as TeleFWI still inverts for relatively smooth velocity variations, the connection to interfaces from RF needs to be better understood through well-designed synthetic experiments.

Joint inversions with ambient-noise data

For regions with both dense linear array and regional 2D arrays, TeleFWI has benefited from joint inversions with ambient noise data (Wang *et al.*, 2021). Although the practice of retrieving empirical Greens functions (EGFs) as another “surface-wave” dataset for tomography has been challenged for nonhomogeneous noise source distributions (e.g., Sager *et al.*, 2020), EGFs have nevertheless been used widely in FWI-based imaging (e.g., Chen *et al.*, 2014; Yang and Gao, 2020). The sensitivity of EGFs to the lithosphere is complementary to that of teleseismic waves and may significantly improve image resolutions at shallow depths. However, joint inversions will inevitably encounter issues of balancing datasets (e.g., body versus surface waves) over multiple iterations and possible inconsistencies arising from fitting two different datasets. Better understanding of the sensitivity of these two datasets and the impact of non-homogeneous source distributions through a combination of synthetic tests and practical data examples may help provide some guidance for joint inversions.

Box tomography

The concept of TeleFWI can be extended to the *Box tomography* (e.g., Clouzet *et al.*, 2018) approach if the imaging target is buried inside the Earth or in-between sources and receivers. Here, the hybrid methods require an additional step to extrapolate the wavefield from the local simulation domain back to the station at the surface for comparison with observed data (Pienkowska *et al.*, 2021). Adaptation in the FWI framework with full-simulation-based Fréchet kernels may be feasible in the near future for array-based local fine-scale imaging of targets such as those in the transition zone or above the core–mantle boundary.

Despite these challenges, TeleFWI may soon become a standard FWI imaging technique applied to dense arrays deployed around the globe, such as those by the Earthscope Primary Instrument Center. With elastic structures mapped to augment images generated by standard array methods, TeleFWI allows more physical interpretation of seismic images and hence help further address the underlying tectonic processes.

DENSE ARRAY, AMBIENT NOISE, AND RESOLVING DETAILED CRUSTAL STRUCTURE (Fan-Chi Lin)

Traditional high-resolution crustal imaging relies on dense recordings of high-frequency seismic signals excited by vibroseis or explosive sources. For such applications, close-spacing geophone sensors are deployed along lines to resolve detailed 2D reflection and refraction profiles. Conversely, passive

seismic tomography studies tend to focus on resolving deeper and larger-scale Earth structures through broadband observations. Despite the less-than-optimal source and receiver distribution, researchers employ first-order approximations and regularizations to linearize and stabilize the inversion problem. Common approximations such as ray approximation and finite-frequency single-scattering approximations work reasonably well when the model perturbation is small.

Despite the general interest in employing passive seismic tomography to resolve crustal structure for applications ranging from energy and resource exploration to geohazard assessment and academic research, constructing high-resolution crustal models can be challenging due to the strong crustal heterogeneity. Notable examples include unconsolidated sediments within major sedimentary basins and partially molten magma reservoirs beneath volcanoes, which can cause seismic velocities to decrease by more than 30% compared to the surrounding bedrock and host rock. Such anomalies can introduce significant wavefield complexities, rendering first-order approximations inaccurate. Numerical tomographic methods (i.e., FWI) have been developed to improve the understanding of the wavefield and iteratively enhance the model constructed (Tromp *et al.*, 2005; Tape *et al.*, 2009). Nonetheless, the creation of a realistic reference starting model remains crucial for achieving rapid convergence and avoiding local minima in the model space.

In contrast to the numerical approach, an alternative approach to improve the understanding of a complex wavefield is to simply improve the receiver coverage. The recent developments in low-cost autonomous geophones have made this approach possible. These can-sized nodal geophones are self-contained, easy to deploy, and can record three-component passive seismic signals for over 30 days in a single deployment. Although these geophone sensors are most sensitive to high-frequency signals, studies have demonstrated their ability to record short-period passive seismic signals relevant to crustal imaging (Wang *et al.*, 2019; Wilgus *et al.*, 2023). As a result, deploying a large- N geophone array has become a practical solution to temporarily enhance data coverage in areas of interest.

Moreover, the deployment of a large- N array combined with the source–receiver duality inherent to the noise cross-correlation method not only improves receiver distribution but also enhances the source distribution. By cross-correlating noise time series recorded by a virtual source station and all other receiver stations across the array, a virtual wavefield can be constructed (Lin *et al.*, 2013). Although various studies have demonstrated the potential for extracting body-wave energy from the noise correlation wavefield (e.g., Nakata *et al.*, 2015; Castellanos *et al.*, 2020), surface waves consistently represent the most energetic and robust signals. Empirical examination of the wavefield and solving the wave equation enable the direct measurement of various local surface-wave properties, including group velocities, phase velocities, local

amplification, and attenuation of Rayleigh and Love waves and Rayleigh-wave ellipticity (Lin *et al.*, 2013, 2014; Bowden *et al.*, 2017). These measurements provide direct constraints on the underlying crustal velocity structure.

Despite the various degrees of success achieved in nodal experiments and ambient noise-based crustal imaging, numerous technical challenges remain to be addressed, offering promising research opportunities. The following is an incomplete list of topics that come to mind, though not intended to be exhaustive or unbiased. First, the characterization of the noise wavefield (i.e., diffusive, semidiffusive, or nondiffusive) is essential for ambient noise applications. Unlike the ubiquitous presence of microseismic noise between 5 and 20 s period, noises at shorter periods are more sensitive to local noise excitation, which is often not well understood. Second, the presence of multimode surface-wave interference can complicate the observed wavefield. The previous studies have demonstrated that higher-mode surface waves can be observed alongside the fundamental mode in areas in major sedimentary environments. Third, shallow crust may exhibit strong anisotropy due to structural foliation and crack alignment, where the often-assumed isotropic structure needs careful examination. Fourth, strong multiscattering is expected near major lateral structural boundaries, and near-field interference between the forward and backscattering waves can be strong.

The pursuit of high-resolution crustal tomographic imaging is advancing through both numerical and empirical approaches. The deployment of large- N geophone arrays combined with ambient noise tomography not only offers significant promise for improving our understanding of Earth's shallow subsurface, but they also come with challenges that demand further research and innovation.

LEVERAGING INTERPRETIVE TOOLS TO BRIDGE TOMOGRAPHY AND GEOLOGY (Eva Golos)

Tomography has the potential to bridge geophysical observations and geologic processes. Other contributions in this work describe efforts toward the goal of quantitative interpretation of tomography that involve direct thermochemical inversion (e.g., Afonso *et al.*, 2016; Fullea *et al.*, 2021). An alternative approach combines seismically determined wavespeed models with forward-modeling to infer thermal, chemical, and rheological properties (Goes and van der Lee, 2002; Cammarano *et al.*, 2009). Implementation of the latter approach is facilitated by the recent development of interpretive toolkits that can be integrated into tomography workflows. To construct a well-posed problem that untangles the effects of multiple processes, these methods require models that constrain multiple geophysical parameters using multiple seismic observations.

One such toolkit is the Whole-Rock Interpretive Seismic Toolbox for Ultramafic Lithologies (WISTFUL; Shinevar *et al.*, 2022). WISTFUL selects the temperature and geochemical composition, defined by major-element oxide content, that

best fit two out of three quantities (V_P , V_S , and V_P/V_S). A correction is applied for the effects of anelasticity, but WISTFUL assumes no melting; so this tool is most appropriate for cratons and other settings where temperatures are well below the solidus. Shinevar *et al.* (2023) apply WISTFUL to determine continental-scale maps of temperature, Mg number, and density from the *MITPS_20* tomography model (Golos *et al.*, 2020). The advantage to fitting temperature and composition from seismic wavespeed, rather than directly inverting seismic data for these properties, is that complicated mineral phase transitions are accounted for, particularly spinel-to-garnet, without needing empirical approximations. In addition, by referencing mantle rock samples, the toolkit restricts interpretation to geologically feasible compositions. Drawbacks of WISTFUL include the absence of hydrated compositions and lack of partial melt modeling.

A second interpretive tool is the very broadband rheology calculator (VBRc; Havlin *et al.*, 2021). This calculator forward-models shear wavespeed and attenuation from temperature, melt fraction, and grain size. Four options are available for modeling anelastic effects on the temperature–velocity relationship. This tool is suitable for active tectonic settings where temperatures approach or exceed the solidus. Hopper *et al.* (2020) utilize VBRc to infer temperature and yield strength of the lithosphere below the East African Rift; Harmon *et al.* (2021) interpret partial melting below the mid-Atlantic ridge from V_S and electrical resistivity structure. One obstacle is that V_S and attenuation are usually supplied by different models, which may differ in spatial resolution. Efforts should be made to use models with comparable spatial resolution, or to jointly invert for velocity and attenuation structure (e.g., Guo and Thurber, 2022). Furthermore, VBRc does not account for geochemical variations.

Because interpretive toolkits gain traction within the community, several challenges must be addressed. Many tomography methods determine percentage perturbations in wavespeed, which must be converted to absolute values. Even models that do report absolute wavespeed are influenced by regularization operations such as damping and smoothing. A recent investigation reports that WISTFUL and VBRc temperature estimates can disagree by as much as $\sim 200^\circ\text{C}$ using the same V_S . In fact, variations on the order of $\sim 100^\circ\text{C}$ exist within VBRc, depending on the choice of anelasticity model. Our understanding of the distribution of attenuation mechanisms, grain size, and melt geometry within the mantle is incomplete, with serious repercussions at the stage of interpretation. The modularization of interpretation within a software package allows mineral physics advances to be readily accommodated within an interpretive framework, without the need to rerun an entire tomographic inversion.

Uncertainty quantification remains a thorny issue. Interpreting geophysical model parameters, themselves obtained by inversion, inherently entails trade-offs. In WISTFUL, V_S is

the most sensitive to temperature (Goes and van der Lee, 2002), whereas V_P/V_S is sensitive to compositional variations as well (Shinevar *et al.*, 2023). In VBRc, attenuation is not highly sensitive to melt fraction, though their relationship cannot be neglected (Havlin *et al.*, 2021). Other geophysical and geochemical methods, including gravity, magnetotellurics, xenoliths, and magma thermobarometry, place further constraints on the parameters of interest.

Publicly available toolkits such as WISTFUL and VBRc offer standardization across studies. If every research group has a proprietary interpretation tool, it is hard to replicate results and compare approaches. Do differences between interpretations arise from the seismic data used, from inversion approach, or from interpretive choices? This question can be addressed if the community coalesces around a set of common tools. Moreover, these toolkits enable interpretation of a wealth of previously determined tomography models to answer geologic questions in myriad locales.

ANISOTROPY FROM CRYSTAL SCALE TO EARTH SCALE (Carl Tape)

Crystals that make up the solid Earth exhibit well-known crystallographic symmetries. Laboratory measurements, such as travel times of ultrasonic seismic waves, can be used to determine the elastic symmetry of crystals (Angel *et al.*, 2009; Almqvist and Mainprice, 2017), and the elastic symmetry may differ from the crystallographic symmetry (Forte and Vianello, 1996). Elasticity is expressed by an elastic mapping $\mathbf{T}(\epsilon) = \sigma$ between 3×3 matrices of strain ϵ and stress σ . The elastic map \mathbf{T} can be represented by a 6×6 symmetric matrix having 21 unique entries. Considering a single crystal, we ask the two questions: (1) What is the measured elastic anisotropy? (2) What is the true elastic anisotropy?

Consider a single crystal of olivine that has orthorhombic crystallographic symmetry and that has elastic symmetry to be determined. In a laboratory setting, it would be the best to measure all 21 elastic parameters, including uncertainties. The measured elastic parameters would almost certainly imply only trivial elastic symmetry, meaning that the only rotational symmetry of \mathbf{T} is the identity matrix. But, within the measurement uncertainties, orthorhombic elastic symmetry might well be a possibility. However, most compilations of single-crystal elastic constants show values (and without uncertainties) that are confined to specific symmetry classes (Almqvist and Mainprice, 2017). An exception would be Brown *et al.* (2016), who list all 21 parameters, with uncertainties, for a set of feldspar crystals.

Anisotropy in the Earth extends to much larger scales, such as a sample of shale rock (Christensen and Mooney, 1995), a crustal metamorphic terrane (Okaya *et al.*, 2004), or a region of uppermost mantle (Maupin and Park, 2007). Toward the future, we can hope for ideal data coverage for making measurements of anisotropy: complete coverage around a laboratory sample of rock, dense (10 m spacing) surface coverage of

seismic sensors along with many fully instrumented boreholes for a kilometer-scale portion of the uppermost crust, dense (10 km spacing) seismic station coverage of the entire planet (land and sea). Recording travel times of waves through these materials enables characterization of the anisotropic structure of the medium. To achieve this, measurements must be taken for all possible paths through each portion of the material, and all measurements must have associated uncertainties. For the estimation side, it would be the best to not assume anything regarding the elastic symmetry of the material, that is, assume trivial symmetry.

For real-Earth seismic imaging, we seldom have ideal coverage, and we are also faced with a highly heterogeneous material. Therefore, we tend to assume that the elastic material has some nontrivial symmetry, such as either isotropic or transverse isotropic with vertical, horizontal, or arbitrary symmetry axis. This reduces the number of unknown parameters at each point in the Earth from 21 to 2, 5, 6, or 7.

Figure 6 provides a framework for visualizing the reductions that are commonly made in seismology and that are implicitly made in compilations of single-crystal elasticity (Almqvist and Mainprice, 2017). Although a true material might have, or be measured to have, trivial symmetry (the ball at the bottom), we might want to assume that the material is isotropic or transversely isotropic (balls at top left). With improvements in data coverage, measurements, computational resources, and algorithms for seismic imaging, we might instead assume that every single crystal in a laboratory and every “cell” in a tomographic model has 21 parameters. With proper handling of measurement uncertainties, these 21 parameters can be estimated from the measurements, and then the question can be asked after the fact: What is the likely elastic symmetry of the material? This approach is currently more tractable at a single-crystal scale, but it seems possible for the future of seismic imaging.

IMPLICATIONS OF VISCOELASTIC RAY THEORY FOR ANELASTIC SEISMIC TOMOGRAPHY (Roger D. Borchardt)

The anelastic conversion of kinetic and potential energy into heat is an important aspect of seismic wave propagation in a layered anelastic Earth. It can be one of the major contributors to larger amounts of apparent attenuation of lower-frequency seismic waves. Inference of the properties and distribution of anelastic Earth materials is fundamental to understanding the internal composition of the Earth (Anderson and Archaubeau, 1966; Romanowicz and Mitchell, 2015).

Standard anelastic models provide valuable estimates of the Earth’s anelastic structure as inferred from average estimates of attenuation along ray paths predicted for P and S waves by elastic ray theory. The recent insights provided by viscoelastic ray theory predict that P and S waves refract across anelastic boundaries with contrasts in anelastic material absorption as inhomogeneous waves with corresponding changes in the

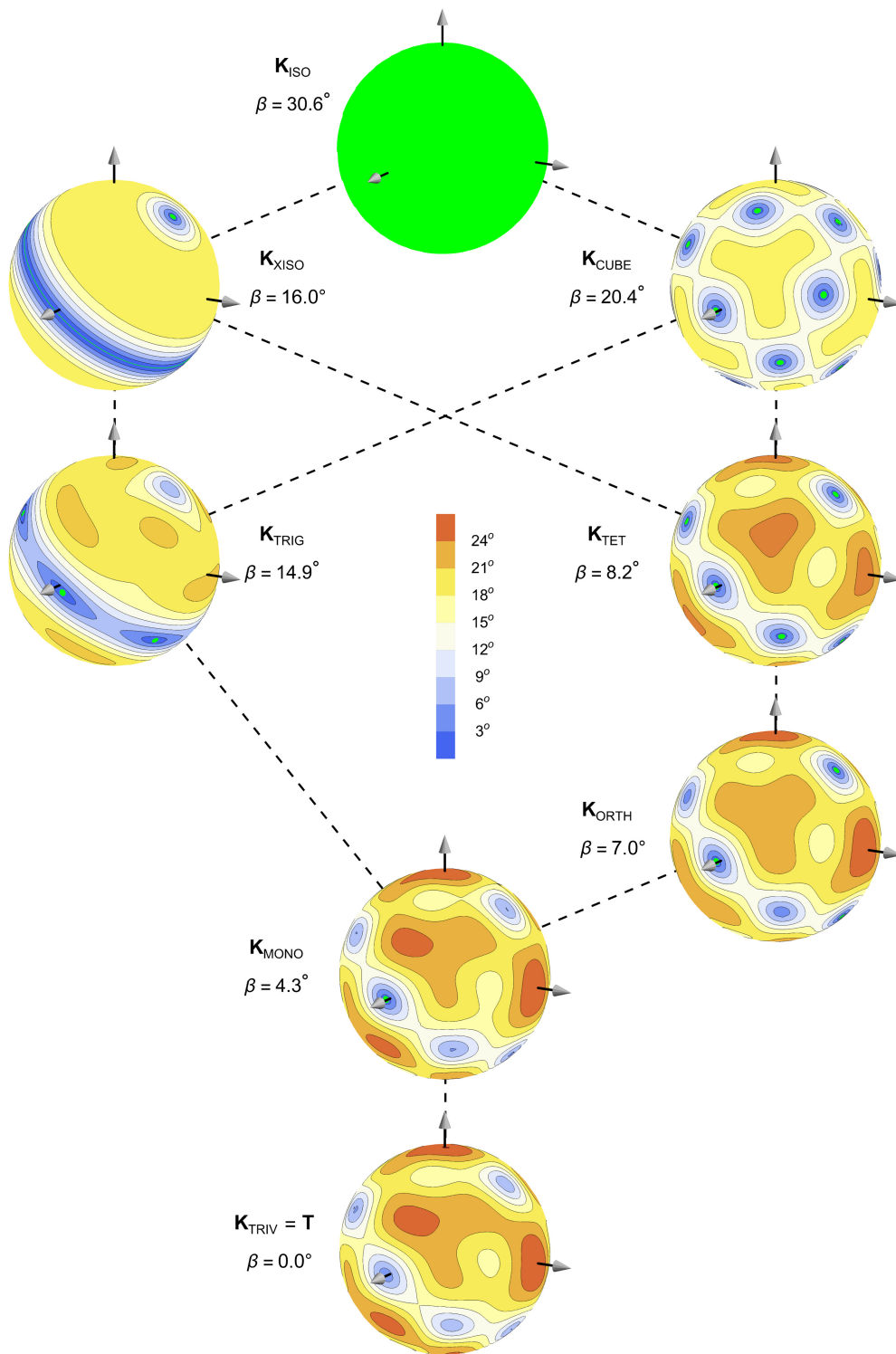


Figure 6. An elastic map \mathbf{T} and the closest map \mathbf{K}_Σ to it having symmetry Σ (trivial, monoclinic, orthorhombic, tetragonal, trigonal, cubic, transversely isotropic, and isotropic). Each map $\mathbf{K} = \mathbf{K}_\Sigma$ is depicted as the contour map of its “monoclinic angle function” $\alpha_{\text{MONO}}^{\mathbf{K}}$ (Tape and Tape, 2022). For a point \mathbf{v} on the sphere, $\alpha_{\text{MONO}}^{\mathbf{K}}(\mathbf{v})$ is the angle between \mathbf{K} and the closest elastic map to \mathbf{K} having a twofold symmetry axis at \mathbf{v} . The green points are where $\alpha_{\text{MONO}}^{\mathbf{K}} = 0$ (inconsistent with the color scale) and are therefore the twofold axes of \mathbf{K} . They determine the symmetry group of \mathbf{K} , which is also seen in the contour plot itself. In this example, \mathbf{T} has trivial symmetry and is from Igel *et al.* (1995); it is $\beta = 4.3^\circ$ from being monoclinic and is $\beta = 30.6^\circ$ from being isotropic. The color version of this figure is available only in the electronic edition.

wave’s speed, attenuation, and trajectory. To account for these effects on seismic waves, especially in areas with high intrinsic material absorption, full implementation of viscoelastic ray theory is needed. A current challenge is to incorporate the recent developments in viscoelastic wave-propagation and ray theory into tomographic inversion procedures.

Viscoelasticity provides an infinite number of phenomenological constitutive models that can be used to describe linear anelastic material behavior (Bland, 1960; Gurtin and Sternberg, 1962; Volterra, 2005). Its general formulation affords exact anelastic raytracing computation algorithms and general anelastic solutions to many of the monochromatic body- and surface-wave problems of seismology, as well as solutions of simple inverse problems to simultaneously infer intrinsic material velocity and intrinsic anelastic material absorption from simultaneous measurements of travel time and amplitude (Borcherdt, 2020).

In the presence of significant contrasts and amounts of anelasticity, a variety of wave characteristics are modified from those for elastic waves. For example, in an anelastic multilayered medium properties of refracted anelastic P and S waves, such as phase and energy speed, trajectory, particle motion, and amplitude, are predicted to vary with angle of incidence, whereas they are invariant for an elastic medium. Refracted anelastic waves are predicted to travel at slower wavespeeds and refract at steeper angles of incidence than for elastic waves, which results in anelastic ray paths with travel

times and distances distinct from those for elastic waves. In addition, the theoretical solutions predict the existence of two types of anelastic inhomogeneous S waves (SI, SII) with distinct elliptical and linear particle motions and distinct reciprocal quality factors.

Numerical results indicate that an important manifestation of these effects is the refraction of energy across anelastic boundaries as a head wave and as wide angle refracted (WAR) waves (Borcherdt, 2020). These anelastic waves, which are not predicted by elastic ray theory, are confirmed by laboratory measurements and numerical models. Interpretations of the travel times and amplitudes of reflected WAR waves, where they are observable, are expected to provide new insights at major anelastic discontinuities for comparison with those of standard reference models such as PREM (Dziewoński and Anderson, 1981) and ak135 (Kennett *et al.*, 1995).

Near-surface seismic recordings of displacement and volumetric strain provide additional empirical evidence in confirmation of theoretically predicted characteristics of anelastic seismic waves (Borcherdt *et al.*, 1989). In general, they confirm that the largest differences between anelastic and elastic waves in layered media occur for near-critical and wide angles of incidence. For precritical angles of incidence they confirm that notable differences in amplitude exist, but travel-time differences are small and well approximated by those inferred for elastic seismic models.

In the context of the conference theme *Seismic Tomography, What Comes Next?*, the general viscoelastic solutions of the fundamental wave-propagation and ray-theory problems for seismology provide a theoretical framework for anelastic seismic tomography. Viscoelastic computation algorithms readily permit the development of general exact raytracing codes for body waves that account for the effect of anelastic boundaries on the travel times, amplitudes, and trajectories of seismic waves for all angles of incidence, including those for head waves and WAR waves. Their full implementation for horizontal and spherical tomography remains to be completed, but they are expected to reveal new insights regarding the thermochemical structure of the Earth's interior over a range of spatial scales when applied to large exploration and teleseismic datasets.

MULTIPHYSICS ADJOINT TOMOGRAPHY OF PORE-SCALE PHENOMENA (Christina Morency)

For the past decades, adjoint tomography has had tremendous successes for regional (e.g., Tape *et al.*, 2009; Zhu *et al.*, 2015; Tao *et al.*, 2018; Rodgers *et al.*, 2022) and global (e.g., Bozdağ *et al.*, 2016; Lei *et al.*, 2020) applications, due in large part to the development of HPC and effective numerical methods (Komatitsch and Vilotte, 1998; Komatitsch and Tromp, 1999). For reservoir-scale applications, such as oil and gas recovery, geothermal, and carbon storage monitoring, subsurface seismic imaging techniques have (1) slowly evolved from purely acoustic to elastic formulations and (2) from focusing on interfaces detections to properties characterization.

In each of these reservoir-scale applications, fluid circulation in a porous and sometimes fractured medium is involved, and the main goal of subsurface imaging is to be able to track, monitor, and characterize pore-fluid properties and fracture networks. Common approaches for subsurface imaging rely predominantly on seismic techniques using acoustic or elastic rheologies, which alone do not directly capture pore fluid properties and related mechanisms. Using Gassmann's formulae (Gassmann, 1951), which relate effective bulk and shear moduli of dry rock to effective moduli of the same rock saturated with fluid, one can only approximate some fluid properties and, in essence, still remain in a seismic elastic paradigm. Even a full seismic poroelastic adjoint approach based on Biot's formulation (Biot, 1956a,b) does not allow efficient access to fluid properties other than fluid bulk modulus and fluid density (Morency *et al.*, 2011). This is in part, because seismometers measure solid displacements and offer few direct constraints on the fluid phase. Another geophysical technique favored to characterize fluid properties such as resistivity and permeability is based on electromagnetic (EM) methods. EM measurements add direct constraints on the fluid phase, but EM signals alone do not offer information on the rock properties. In the last decades, there have been efforts to combine both seismic and EM datasets for exploration geophysics. The most popular approach is based on joint inversion of seismic and EM datasets as decoupled phenomena to recover seismic velocity and electrical resistivity (e.g., Hoversten *et al.*, 2006; Hu *et al.*, 2009; Colombo and Rovetta, 2018).

However, back in the 1930s, Ivanov's observations showed that ground motion triggered by a seismic source propagating in a porous medium generates an electric field due to electrokinetic forces at the pore scale underlying the natural coupling of seismic and EM phenomena (Ivanov, 1939). We have to wait until the 1990s and later for theoretical and experimental development of what are known as the seismoelectric effects, with first field data collected and analyzed by Thompson and Gist (1993), experimental studies by for example, Mikhailov *et al.* (2000), Bordes *et al.* (2015), Martins Gomes (2022), and the rise of numerical modeling supported by Pride's formulation (Pride, 1994) based on the coupled Biot poroelastic seismic and Maxwell electromagnetic wave equations (e.g., Haines and Pride, 2006; Revil and Jardani, 2010; Meyer, 2021; Morency and Matzel, 2021).

A natural next step is tackling the inverse problem. However, existing literature on the inversion of seismoelectric datasets is not extensive. The most notable and, to my knowledge, first work on seismoelectric signal inversion is based on a probabilistic approach, where Jardani *et al.* (2010) developed and conducted a stochastic joint inversion of synthetic seismic and seismoelectric datasets, using an Adaptive Metropolis algorithm. Considering two flat layers plus a rectangular reservoir embedded in the second layer 2D geometry, they were able to recover the permeability within one order of

magnitude; and the electrical conductivity and poroelastic mechanical properties were well resolved, but the porosity was not well constrained. Several studies have focused on sensitivity analysis and impact of SNR, and they show that the inversion of seismoelectric data alone performed better than that of seismic data alone, and that the joint inversion of both seismic and seismoelectric datasets offers the best resolution of electric and poroelastic model parameters (Mahardika *et al.*, 2012; Macchioli-Grande *et al.*, 2020).

Seismoelectric inversion has the potential to combine the resolution and depth of penetration of seismic techniques with the sensitivity of EM techniques to pore-fluid properties. I believe that the adjoint method can be as big a game changer for seismoelectric signals inversion, as it has been for seismic tomography. That is why the work by Morency and Matzel (2021) based on an SEM to resolve seismoelectric effects is forging the path toward joint adjoint inversion of seismic and electric properties using seismoelectric datasets, leveraging the SPECFEM package and the previous work on adjoint seismic tomography. There is still a lot of room for research on seismoelectric data acquisition, processing, and inversion to demonstrate practical use of this technique (Morency *et al.*, 2022), which should keep on opening the future areas of work on these exciting pore-scale phenomena.

CONCLUSIONS

Seismic Tomography 2023 offers a snapshot of modern seismic tomography with a focus on outstanding challenges and particularly promising research directions. Written by an experienced group of authors, it is intended to guide not only other Earth science professionals but also young students who wish to develop their own research in this exciting field.

Although a superficial look at the individual contributions may give the impression that their topics are scattered and disconnected, a more careful read reveals a small number of coherent threads. The diversity is only apparent, and often topics are just seen from different angles, influenced by personal preferences and variable experience.

Simply counting how often a topic is mentioned, possibly in different disguises, the most prominent challenges seem to be two closely related classics: (1) data quality and quantity, especially in the oceans and the southern-hemisphere continents, and (2) multiparameter inversion in a broader sense, including not only anisotropy and attenuation but also poroelastic parameters. Clearly, (1) is the most obvious, though certainly not the easiest, approach to making progress on (2).

Several other frequently mentioned topics can be understood in the context of these two: (3) Multiparameter inversion increases the importance of interparameter trade-offs, thereby amplifying the need for careful uncertainty quantification. Despite major efforts, uncertainty quantification is still considered by many an open problem not only due to limited computational resources but also partly because rather technical

uncertainty proxies may not be particularly useful in geologic interpretations. (4) Reformulation of tomographic problems so that hypothesis testing of geological and geodynamic issues replaces comprehensive uncertainty quantification that is often infeasible in practice. (5) Further advancing FWI to optimally exploit information in seismic recordings is considered one of the most promising approaches toward multiparameter inversion and the reduction of uncertainties. The most critical advance is the increase of frequency bandwidth, and related developments in numerical wave propagation, HPC, and nonlinear optimization. (6) Last but not the least, the future progress in seismic tomography hinges on more careful presentations of our models to facilitate quantitative comparisons. Although uncertainty quantification would be an important step toward a better comparability of models, there may be much more low-hanging fruit, including the presentation of absolute seismic wavespeeds, the omission of the 210 km discontinuity from initial models, or the low-pass filtering of different models to produce images of comparable spatial resolution.

This article should be interpreted as a document of its time and a reference point for the future developments. It remains to be seen which of the major problems will be considered solved, to some extent, in *Seismic Tomography 2033*.

DATA AND RESOURCES

There are no new data or resources to report for this article.

DECLARATION OF COMPETING INTERESTS

The authors acknowledge that there are no conflicts of interest recorded.

ACKNOWLEDGMENTS

The authors gratefully acknowledge invaluable support provided by the Seismological Society of America, and, in particular, by Nan Broadbent and Rikki Anderson, during the organization of the 2022 Seismic Tomography conference in Toronto. Countless discussions and interesting presentations made the meeting a real success. Contribution of A. R. and C. M. prepared by LLNL under Contract Number DE-AC52-07NA27344. E. B. acknowledges the support by the National Science Foundation (NSF) under Award Number EAR1945565 and the Texas Advanced Computing Center (TACC) at the University of Texas at Austin for providing computational resources on the Frontera system (Stanzione *et al.*, 2020) through allocation EAR21003 (www.tacc.utexas.edu, last accessed April 2024). S. L. acknowledges support from the Natural Environment Research Council (NERC), UK, under Grant Number XE/X000060/1. V. C. T. acknowledges support from National Science Foundation (NSF) Grant Number EAR-2011079. C. T. was supported by National Science Foundation Grant Number EAR 2342129.

REFERENCES

Adourian, S., C. Lyu, Y. Masson, F. Munch, and B. Romanowicz (2021). Combining different 3D global and regional seismic wave propagation solvers towards box tomography in the deep earth, *Geophys. J. Int.* **232**, 1340–1356.

- Afanasyev, M., C. Boehm, M. van Driel, L. Krischer, M. Rietmann, D. A. May, M. G. Knepley, and A. Fichtner (2019). Modular and flexible spectral-element waveform modelling in two and three dimensions, *Geophys. J. Int.* **216**, no. 3, 1675–1692, doi: [10.1093/gji/ggy469](https://doi.org/10.1093/gji/ggy469).
- Afonso, J. C., N. Rawlinson, Y. Yang, D. L. Schutt, A. G. Jones, J. Fulla, and W. L. Griffin (2016). 3-D multiobservable probabilistic inversion for the compositional and thermal structure of the lithosphere and upper mantle: III. Thermochemical tomography in the western-central U.S., *J. Geophys. Res.* **121**, no. 10, 7337–7370, doi: [10.1002/2016JB013049](https://doi.org/10.1002/2016JB013049).
- Aki, K., and W. H. K. Lee (1976). Determination of three-dimensional velocity anomalies under a seismic array using first P arrival times from local earthquakes—I. A homogeneous initial model, *J. Geophys. Res.* **81**, 4381–4399, doi: [10.1029/JB081i023p04381](https://doi.org/10.1029/JB081i023p04381).
- Aki, K., A. Christoffersson, and E. S. Husebye (1977). Determination of three-dimensional seismic structure of the lithosphere, *J. Geophys. Res.* **81**, 277–296, doi: [10.1029/JB082i002p00277](https://doi.org/10.1029/JB082i002p00277).
- Almqvist, B. S. G., and D. Mainprice (2017). Seismic properties and anisotropy of the continental crust: Predictions based on mineral texture and rock microstructure, *Rev. Geophys.* **55**, 367–433, doi: [10.1002/2016RG000552](https://doi.org/10.1002/2016RG000552).
- Anderson, D. L. (1967). The anelasticity of the mantle, *Geophys. J. Roy. Astron. Soc.* **14**, 135–164.
- Anderson, D. L., and C. B. Archambeau (1966). The anelasticity of the Earth, *J. Geophys. Res.* **69**, 2071–2084.
- Angel, R. J., J. M. Jackson, H. J. Reichmann, and S. Speziale (2009). Elasticity measurements on minerals: a review, *Eur. J. Mineral.* **21**, 525–550, doi: [10.1127/0935-1221/2009/0021-1925](https://doi.org/10.1127/0935-1221/2009/0021-1925).
- Austermann, J., J. X. Mitrovica, K. Latychev, and G. A. Milne (2013). Barbados-based estimate of ice volume at last glacial maximum affected by subducted plate, *Nature Geosci.* **6**, 553–557.
- Bachmann, E., and J. Tromp (2020). Source encoding for viscoacoustic ultrasound computed tomography, *J. Acoust. Soc. Am.* **147**, no. 5, 3221–3235.
- Backus, G. E., and F. Gilbert (1970). Uniqueness in the inversion of inaccurate gross Earth data, *Phil. Trans. Roy. Soc. London* **266**, 123–192.
- Bamberger, A., G. Chavent, and P. Lailly (1977). Une application de la théorie du contrôle à un problème inverse sismique, *Ann. Geophys.* **33**, 183–200.
- Bartzsch, S., S. Lebedev, and T. Meier (2011). Resolving the lithosphere-asthenosphere boundary with seismic Rayleigh waves, *Geophys. J. Int.* **186**, no. 3, 1152–1164.
- Beller, S., V. Monteiller, S. Operto, G. Nolet, A. Paul, and L. Zhao (2018). Lithospheric architecture of the south-western Alps revealed by multiparameter teleseismic full-waveform inversion, *Geophys. J. Int.* **212**, 1369–1388.
- Ben-Hadj-Ali, H., S. Operto, and J. Virieux (2009). An efficient frequency-domain full waveform inversion method using simultaneous encoded sources, *Geophysics* **76**, R109–R124.
- Bernauer, M., A. Fichtner, and H. Igel (2014). Optimal observables for multiparameter seismic tomography, *Geophys. J. Int.* **198**, 1241–1254.
- Betancourt, M. (2017). A conceptual introduction to Hamiltonian Monte Carlo, available at <https://arxiv.org/abs/1701.02434> (last accessed April 2024).
- Bianchi, M. B., M. Assumpção, M. P. Rocha, J. M. Carvalho, P. A. Azevedo, S. L. Fontes, F. L. Dias, J. M. Ferreira, A. F. Nascimento, M. V. Ferreira, *et al.* (2018). The Brazilian Seismographic Network (RSBR): Improving seismic monitoring in Brazil, *Seismol. Res. Lett.* **89**, 452–457, doi: [10.1785/0220170227](https://doi.org/10.1785/0220170227).
- Bijwaard, H., W. Spakman, and E. R. Engdahl (1998). Closing the gap between regional and global traveltimes tomography, *J. Geophys. Res.* **103**, 30,055–30,078.
- Biot, M. A. (1956a). Theory of propagation of elastic waves in a fluid-saturated porous solid. II. Higher frequency range, *J. Acoust. Soc. Am.* **28**, 179–191.
- Biot, M. A. (1956b). Theory of propagation of elastic waves in a fluid-saturated porous solid. I. Low-frequency range, *J. Acoust. Soc. Am.* **28**, 168–178.
- Bland, D. R. (1960). *The Theory of Linear Viscoelasticity*, Pergamon Press, New York.
- Bodin, T., and M. Sambridge (2009). Seismic tomography with the reversible jump algorithm, *Geophys. J. Int.* **178**, 1411–1436.
- Bodin, T., M. Sambridge, N. Rawlinson, and P. Arroucau (2012). Transdimensional tomography with unknown data noise, *Geophys. J. Int.* **189**, 1536–1556.
- Bonadio, R., S. Lebedev, T. Meier, P. Arroucau, A. J. Schaeffer, A. Licciardi, M. R. Agius, C. Horan, L. Collins, B. M. O'Reilly, *et al.* (2021). Optimal resolution tomography with error tracking and the structure of the crust and upper mantle beneath Ireland and Britain, *Geophys. J. Int.* **226**, no. 3, 2158–2188.
- Borcherdt, R. D. (2020). *Viscoelastic Waves and Rays in Layered Media*, Cambridge University Press, Cambridge, United Kingdom.
- Borcherdt, R. D. (2024). Preliminary implications of viscoelastic ray theory for anelastic seismic tomography models, *Bull. Seismol. Soc. Am.* doi: [10.1785/0120230226](https://doi.org/10.1785/0120230226).
- Borcherdt, R. D., M. J. S. Johnston, and G. Glassmoyer (1989). On the use of volumetric strain meters to infer additional characteristics of short-period seismic radiation, *Bull. Seismol. Soc. Am.* **79**, 1006–1023.
- Bordes, C., P. Sénéchal, J. Barrière, D. Brito, E. Normandin, and D. Jougnot (2015). Impact of water saturation on seismoelectric transfer functions: A laboratory study of coseismic phenomenon, *Geophys. J. Int.* **200**, no. 3, 1317–1335.
- Bowden, D. C., V. C. Tsai, and F.-C. Lin (2017). Amplification and attenuation across USArray using ambient noise waveform tracking, *J. Geophys. Res.* **122**, doi: [10.1002/2017JB014804](https://doi.org/10.1002/2017JB014804).
- Bozdağ, E., D. Peter, M. Lefebvre, D. Komatitsch, J. Tromp, J. Hill, N. Podhorszki, and D. Pugmire (2016). Global adjoint tomography: First-generation model, *Geophys. J. Int.* **207**, no. 3, 1739–1766.
- Brown, J. M., R. J. Angel, and N. L. Ross (2016). Elasticity of plagioclase feldspars, *J. Geophys. Res.* **121**, 663–675, doi: [10.1002/2015JB012736](https://doi.org/10.1002/2015JB012736).
- Bunge, H.-P., and M. A. Richards (1996). The origin of large scale structure in mantle convection: Effects of plate motions and viscosity stratification, *Geophys. Res. Lett.* **23**, 2987–2990.
- Cammarano, F., B. Romanowicz, L. Stixrude, C. Lithgow-Bertelloni, and W. Xu (2009). Inferring the thermochemical structure of the upper mantle from seismic data, *Geophys. J. Int.* **179**, no. 2, 1169–1185.
- Cammarano, F., P. Tackley, and L. Boschi (2011). Seismic, petrological and geodynamical constraints on thermal and compositional structure of the upper mantle: Global thermochemical models, *Geophys. J. Int.* **187**, 1301–1318.

- Capdeville, Y., C. Larmat, J. P. Vilotte, and J. P. Montagner (2002). A new coupled spectral element and modal solution method for global seismology: A first application to the scattering induced by a plume-like anomaly, *Geophys. Res. Lett.* **29**, 32-1–32-4, doi: [10.1029/2001GL013747](https://doi.org/10.1029/2001GL013747).
- Carmona, A. E., D. Peter, L. Parisi, and P. M. Mai (2024). Anelastic tomography of the Arabian plate, *Bull. Seismol. Soc. Am.* doi: [10.1785/0120230216](https://doi.org/10.1785/0120230216).
- Castellanos, C., L. Métivier, S. Operto, R. Brossier, and J. Virieux (2015). Fast full waveform inversion with source encoding and second-order optimization methods, *Geophys. J. Int.* **200**, 718–742.
- Castellanos, J., R. Clayton, and A. Juarez (2020). Using a time-based subarray method to extract and invert noise-derived body waves at Long Beach, California, *J. Geophys. Res.* **125**, no. 5, e2019JB018855, doi: [10.1029/2019JB018855](https://doi.org/10.1029/2019JB018855).
- Castelvecchi, D. (2017). Long-awaited mathematics proof could help scan Earth's innards, *Nature* **542**, 281–282.
- Chaves, C. A. M., J. Ritsema, and P. Koelemeijer (2020). Comparing ray-theoretical and finite-frequency teleseismic travel times: Implications for constraining the ratio of s-wave to p-wave velocity variations in the lower mantle, *Geophys. J. Int.* **224**, 1540–1552, doi: [10.1093/gji/ggaa534](https://doi.org/10.1093/gji/ggaa534).
- Chen, M., H. Huang, H. J. Yao, R. D. van der Hilst, and F. L. Niu (2014). Low wave speed zones in the crust beneath SE Tibet revealed by ambient noise adjoint tomography, *Geophys. Res. Lett.* **41**, 334–340.
- Choi, Y., and T. Alkhalifah (2011). Source-independent time-domain wave-form inversion using convolved wavefields, *Geophysics* **76**, R125–R134.
- Chow, B., Y. Kaneko, C. Tape, R. Modrak, and J. Townend (2020). An automated workflow for adjoint tomography—Waveform misfits and synthetic inversions for the North Island, New Zealand, *Geophys. J. Int.* **223**, no. 3, 1461–1480, doi: [10.1093/gji/ggaa381](https://doi.org/10.1093/gji/ggaa381).
- Christensen, N. I., and W. D. Mooney (1995). Seismic velocity structure and composition of the continental crust: A global view, *J. Geophys. Res.* **100**, no. B7, 9761–9788.
- Civiero, C., S. Lebedev, Y. Xu, R. Bonadio, and F. Lavoué (2024). Toward tectonic-type and global 1D seismic models of the upper mantle constrained by broadband surface waves, *Bull. Seismol. Soc. Am.* doi: [10.1785/0120230295](https://doi.org/10.1785/0120230295).
- Clouzet, P., Y. Masson, and B. Romanowicz (2018). Box tomography: First application to the imaging of upper-mantle shear velocity and radial anisotropy structure beneath the North American continent, *Geophys. J. Int.* **213**, 1849–1875.
- Colombo, D., and D. Rovetta (2018). Coupling strategies in multiparameter geophysical joint inversion, *Geophys. J. Int.* **215**, no. 2, 1171–1184.
- Connolly, J. A. (2005). Computation of phase equilibria by linear programming: A tool for geodynamic modeling and its application to subduction zone decarbonation, *Earth Planet. Sci. Lett.* **236**, nos. 1/2, 524–541.
- Cottaar, S., and V. Lekic (2016). Morphology of seismically slow lower-mantle structures, *Geophys. J. Int.* **207**, 1122–1136.
- Cui, C., E. Bachmann, D. Peter, Z. Liu, and J. Tromp (2023). Source-encoded waveform inversion of the Northern Hemisphere, *Geophys. J. Int.* **235**, 2305–2322, doi: [10.1093/gji/ggad363](https://doi.org/10.1093/gji/ggad363).
- Cupillard, P., E. Delavaud, G. Burgos, G. Festa, J.-P. Vilotte, Y. Capdeville, and J.-P. Montagner (2012). RegSEM: A versatile code based on the spectral element method to compute seismic wave propagation at the regional scale, *Geophys. J. Int.* **188**, 1203–1220.
- Dahlen, F. A., S.-H. Hung, and G. Nolet (2000). Fréchet kernels for finite-frequency travel times – I. Theory, *Geophys. J. Int.* **141**, 157–174.
- Dahlen, F. A., and J. Tromp (1998). *Theoretical Global Seismology*, Princeton University Press, New Jersey.
- Dalton, C. A., G. Ekström, and A. M. Dziewonski (2008). The global attenuation structure of the upper mantle, *J. Geophys. Res.* **113**, doi: [10.1029/2007JB005429](https://doi.org/10.1029/2007JB005429).
- de Jong, J. H. E., H. Paulssen, T. van Leeuwen, and J. Trampert (2022). Sensitivity kernels for receiver function misfits in a full waveform inversion workflow, *Geophys. J. Int.* **230**, 1065–1079, doi: [10.1093/gji/ggac098](https://doi.org/10.1093/gji/ggac098).
- Debayle, E., and Y. Ricard (2012). A global shear velocity model of the upper mantle from fundamental and higher Rayleigh mode measurements, *J. Geophys. Res.* doi: [10.1029/2012JB009288](https://doi.org/10.1029/2012JB009288).
- Del Piccolo, G., B. P. Vanderbeek, M. Faccenda, A. Morelli, and J. Byrnes (2024). Imaging upper mantle anisotropy with trans-dimensional Bayesian Monte Carlo sampling, *Bull. Seismol. Soc. Am.* doi: [10.1785/0120230233](https://doi.org/10.1785/0120230233).
- Donini, A., S. Palomares-Ruiz, and J. Salvado (2019). Neutrino tomography of Earth, *Nature Phys.* **15**, 37–40.
- Duane, S., A. D. Kennedy, B. J. Pendleton, and D. Roweth (1987). Hybrid Monte Carlo, *Phys. Lett. B* **195**, 216–222.
- Durek, J. J., and G. Ekström (1996). A radial model of anelasticity consistent with long-period surface wave attenuation, *Bull. Seismol. Soc. Am.* **86**, 144–158.
- Dziewonski, A. M. (1984). Mapping the lower mantle: Determination of lateral heterogeneity in p velocity up to degree and order 6, *J. Geophys. Res.* **89**, 5929–5952.
- Dziewoński, A. M., and D. L. Anderson (1981). Preliminary reference earth model, *Phys. Earth Planet. In.* **25**, 297–356, doi: [10.1016/0031-9201\(81\)90046-7](https://doi.org/10.1016/0031-9201(81)90046-7).
- Dziewonski, A. M., and D. L. Anderson (1984). Seismic Tomography of the Earth's Interior: The first three-dimensional models of the earth's structure promise to answer some basic questions of geodynamics and signify a revolution in earth science, *Am. Sci.* **72**, 483–494.
- Dziewoński, A. M., B. H. Hager, and R. J. O'Connell (1977). Large-scale heterogeneities in the lower mantle, *J. Geophys. Res.* **82**, 239–255.
- Eberhart-Phillips, D., and B. Fry (2017). A new scheme for joint surface wave and earthquake travel-time inversion and resulting 3-D velocity model for the western North Island, New Zealand, *Phys. Earth Planet. In.* **269**, 98–111, doi: [10.1016/j.pepi.2017.05.014](https://doi.org/10.1016/j.pepi.2017.05.014).
- Ekström, G., and A. M. Dziewonski (1998). The unique anisotropy of the Pacific upper mantle, *Nature* **394**, 168–172.
- Eppinger, B. J., W. S. Holbrook, Z. Liu, B. A. Flinchum, and J. Tromp (2024). Near-surface full-waveform inversion reveals bedrock controls on critical zone architecture, *J. Geophys. Res.* **11**, e2023EA003248, doi: [10.1029/2023EA003248](https://doi.org/10.1029/2023EA003248).
- Fang, H., R. D. van der Hilst, M. V. de Hoop, K. Kothari, S. Gupta, and I. Dokmanić (2019). Parsimonious seismic tomography with

- Poisson Voronoi projections: Methodology and validation, *Seism. Res. Lett.* **91**, no. 1, 343–355, doi: [10.1785/0220190141](https://doi.org/10.1785/0220190141).
- Fang, H., H. Zhang, H. Yao, A. Allam, D. Zigone, Y. Ben-Zion, C. Thurber, and R. D. van der Hilst (2016). A new algorithm for three-dimensional joint inversion of body wave and surface wave data and its application to the southern California plate boundary region, *J. Geophys. Res.* **121**, 3557–3569, doi: [10.1002/2015JB012702](https://doi.org/10.1002/2015JB012702).
- Fichtner, A. (2010). *Full Seismic Waveform Modelling and Inversion*, Springer, Heidelberg.
- Fichtner, A., and J. Trampert (2011). Hessian kernels of seismic data functionals based upon adjoint techniques, *Geophys. J. Int.* **185**, 775–798.
- Fichtner, A., H.-P. Bunge, and H. Igel (2006). The adjoint method in seismology: I. Theory, *Phys. Earth Planet. In.* **157**, no. 1, 86–104, doi: [10.1016/j.pepi.2006.03.016](https://doi.org/10.1016/j.pepi.2006.03.016).
- Fichtner, A., B. L. N. Kennett, H. Igel, and H.-P. Bunge (2009). Full seismic waveform tomography for upper-mantle structure in the Australasian region using adjoint methods, *Geophys. J. Int.* **179**, 1703–1725.
- Fichtner, A., D. P. van Herwaarden, M. Afanasiev, S. Simutè, L. Krischer, Y. Çubuk-Sabuncu, T. Taymaz, L. Colli, E. Saygin, A. Villaseñor, *et al.* (2018). The collaborative seismic earth model: Generation I, *Geophys. Res. Lett.* **45**, 4007–4016.
- Fichtner, A., and A. Zunino (2019). Hamiltonian nullspace shuttles, *Geophys. Res. Lett.* **46**, 644–651.
- Fichtner, A., A. Zunino, and L. Gebraad (2019). Hamiltonian Monte Carlo solution of tomographic inverse problems, *Geophys. J. Int.* **216**, 1344–1363, doi: [10.1093/gji/ggy496](https://doi.org/10.1093/gji/ggy496).
- Forte, S., and M. Vianello (1996). Symmetry classes for elasticity tensors, *J. Elasticity* **43**, 81–108.
- French, S. W., and B. A. Romanowicz (2014). Whole-mantle radially anisotropic shear velocity structure from spectral-element waveform tomography, *Geophys. J. Int.* **199**, 1303–1327.
- French, S. W., and B. A. Romanowicz (2015). Broad plumes rooted at the base of the Earth's mantle beneath major hotspots, *Nature* **525**, 1303–1327.
- Fullea, J., S. Lebedev, M. Agius, A. Jones, and J. C. Afonso (2012). Lithospheric structure in the Baikal-central Mongolia region from integrated geophysical-petrological inversion of surface-wave data and topographic elevation, *Geochem. Geophys. Geosys.* **13**, no. 8, doi: [10.1029/2012GC004138](https://doi.org/10.1029/2012GC004138).
- Fullea, J., S. Lebedev, Z. Martinec, and N. Celli (2021). WINTERC-G: Mapping the upper mantle thermochemical heterogeneity from coupled geophysical-petrological inversion of seismic waveforms, heat flow, surface elevation and gravity satellite data, *Geophys. J. Int.* **226**, no. 1, 146–191.
- Gassmann, F. (1951). Über die Elastizität poröser Medien, *Vier der Natur Gesellschaft in Zurich* **96**, 1–23 (in German).
- Goes, S., and S. van der Lee (2002). Thermal structure of the North American uppermost mantle inferred from seismic tomography, *J. Geophys. Res.* **107**, no. B3, ETG 2-1–ETG 2-13, doi: [10.1029/2000JB000049](https://doi.org/10.1029/2000JB000049).
- Golos, E. M., H. Fang, and R. D. van der Hilst (2020). Variations in seismic wave speed and VP/VS ratio in the North American lithosphere, *J. Geophys. Res.* **125**, no. 12, e2020JB020574, doi: [10.1029/2020JB020574](https://doi.org/10.1029/2020JB020574).
- Gorbatov, A., and B. L. N. Kennett (2003). Joint bulk-sound and shear tomography for western Pacific subduction zones, *Earth Planet. Sci. Lett.* **210**, 527–543.
- Guo, H., and C. Thurber (2022). Temporal changes in seismic velocity and attenuation at The Geysers geothermal field, California, from double-difference tomography, *J. Geophys. Res.* **127**, no. 5, e2021JB022938, doi: [10.1029/2021JB022938](https://doi.org/10.1029/2021JB022938).
- Guo, Z., and Y. Zhou (2019). Finite-frequency imaging of the global 410- and 660-km discontinuities using SS precursors, *Geophys. J. Int.* **220**, 1978–1994.
- Gurtin, M. E., and E. Sternberg (1962). On the linear theory of viscoelasticity, in *Archive for Rational Mechanics and Analysis*, Vol. 11, 291–356.
- Haines, S. S., and S. R. Pride (2006). Seismoelectric numerical modeling on a grid, *Geophysics* **71**, no. 6, N57–N65.
- Haney, M. M., and V. C. Tsai (2015). Nonperturbational surface-wave inversion: A Dix-type relation for surface waves, *Geophysics* **80**, EN167–EN177.
- Haney, M. M., and V. C. Tsai (2017). Perturbational and nonperturbational inversion of Rayleigh-wave velocities, *Geophysics* **82**, F15–F28.
- Harmon, N., S. Wang, C. A. Rychert, S. Constable, and J. M. Kendall (2021). Shear velocity inversion guided by resistivity structure from the PI-LAB experiment for integrated estimates of partial melt in the mantle, *J. Geophys. Res.* **126**, no. 8, e2021JB022202, doi: [10.1029/2021JB022202](https://doi.org/10.1029/2021JB022202).
- Havlin, C., B. K. Holtzman, and E. Hopper (2021). Inference of thermodynamic state in the asthenosphere from anelastic properties, with applications to North American upper mantle, *Phys. Earth Planet. In.* **314**, 106639, doi: [10.1016/j.pepi.2020.106639](https://doi.org/10.1016/j.pepi.2020.106639).
- Hawkins, R., M. Khalid, K. Smetana, and J. Trampert (2023). Model order reduction for seismic waveform modelling: Inspiration from normal modes, *Geophys. J. Int.* **234**, no. 3, 2255–2283.
- Hopper, E., J. B. Gaherty, and D. J. Shillington (2020). Preferential localized thinning of lithospheric mantle in the melt-poor Malawi Rift, *Nature Geosci.* **13**, 584–589, doi: [10.1038/s41561-020-0609-y](https://doi.org/10.1038/s41561-020-0609-y).
- Hosseini, K., K. J. Matthews, K. Sigloch, G. E. Shephard, M. Domeier, and M. Tsekhmistrenko (2018). Submachine: Web-based tools for exploring seismic tomography and other models of Earth's deep interior, *Geochem. Geophys. Geosys.* **19**, 1464–1483.
- Hoversten, G. M., F. Cassasuce, E. Gasperikova, G. A. Newman, J. Chen, Y. Rubin, Z. Hou, and D. Vasco (2006). Direct reservoir parameter estimation using joint inversion of marine seismic AVA and CSEM data, *Geophysics* **71**, no. 3, C1–C13, doi: [10.1190/1.2194510](https://doi.org/10.1190/1.2194510).
- Hu, W., A. Abubakar, and T. M. Habashy (2009). Joint electromagnetic and seismic inversion using structural constraints, *Geophysics* **74**, no. 6, R99–R109.
- Huang, Y., and G. Schuster (2012). Multisource least-squares migration of marine streamer and land data with frequency-division encoding, *Geophys. Prospect.* **60**, 663–680.
- Huang, Y., and G. Schuster (2017). Multisource full waveform inversion of marine streamer data with frequency selection, *Geophys. Prospect.* **66**, 1243–1257, doi: [10.1111/1365-2478.12588](https://doi.org/10.1111/1365-2478.12588).
- Igel, H., P. Mora, and B. Rioulet (1995). Anisotropic wave propagation through finite-difference grids, *Geophysics* **60**, no. 4, 1203–1216.

- Incorporated Research Institutions for Seismology (IRIS) (2018). Data services newsletter, Vol. 20, no. 1, available at <https://ds.iris.edu/ds/newsletter/vol20/no1/> (last accessed July 2023).
- Ivanov, A. G. (1939). Effect of electrization of Earth layers waves passing through them, *Dokl. Akad. Nauk. SSSR* **24**, 42–45.
- Iyer, H. M., and K. Hirahara (1993). *Seismic Tomography, Theory and Practice*, Chapman and Hall, London.
- Jackson, D. D. (1972). Interpretation of inaccurate, insufficient and inconsistent data, *Geophys. J. Roy. Astron. Soc.* **28**, 97–109.
- Jardani, A., A. Revil, E. Slod, and W. Söllner (2010). Stochastic joint inversion of 2D seismic and seismoelectric signals in linear poroelastic materials: A numerical investigation, *Geophysics* **75**, N19–N31.
- Kan, L. Y., S. Chevrot, and V. Monteiller (2023). Dehydration of the subducting Juan de Fuca plate and fluid pathways revealed by full waveform inversion of teleseismic P and SH waves in central Oregon, *J. Geophys. Res.* **128**, e2022JB025506, doi: [10.1029/2022JB025506](https://doi.org/10.1029/2022JB025506).
- Kanamori, H., and D. L. Anderson (1977). Importance of physical dispersion in surface wave and free oscillation problems: Review, *Rev. Geophys.* **15**, no. 1, 105–112, doi: [10.1029/RG015i001p00105](https://doi.org/10.1029/RG015i001p00105).
- Karaoğlu, H., and B. Romanowicz (2018). Inferring global upper-mantle shear attenuation structure by waveform tomography using the spectral element method, *Geophys. J. Int.* **213**, 1536–1558.
- Karato, S.-I., and H. Jung (1998). Water, partial melting and the origin of the seismic low velocity and high attenuation zone in the upper mantle, *Earth Planet. Sci. Lett.* **157**, 193–207.
- Karato, S.-I., and B. B. Karki (2001). Origin of lateral variation of seismic wave velocities and density in the deep mantle, *J. Geophys. Res.* **106**, 21,771–21,783, doi: [10.1029/2001JB000214](https://doi.org/10.1029/2001JB000214).
- Kennett, B. L. N., and M. Sambridge (1998). Inversion for multiple parameter classes, *Geophys. J. Int.* **135**, no. 1, 304–306, doi: [10.1046/j.1365-246X.1998.00657.x](https://doi.org/10.1046/j.1365-246X.1998.00657.x).
- Kennett, B. L. N., E. R. Engdahl, and R. Buland (1995). Constraints on seismic velocities in the Earth from travel times, *Geophys. J. Int.* **122**, 108–124.
- Kennett, B. L. N., S. Widiyantoro, and R. van der Hilst (1998). Joint seismic tomography for bulk-sound and shear wave speed in the Earth's mantle, *J. Geophys. Res.* **103**, 12,469–12,493.
- Komatitsch, D., and J. Tromp (1999). Introduction to the spectral element method for three-dimensional seismic wave propagation, *Geophys. J. Int.* **139**, 806822, doi: [10.1046/j.1365-246x.1999.00967.x](https://doi.org/10.1046/j.1365-246x.1999.00967.x).
- Komatitsch, D., and J. Tromp (2002). Spectral-element simulations of global seismic wave propagation, Part I: Validation, *Geophys. J. Int.* **149**, 390–412.
- Komatitsch, D., and J. P. Vilotte (1998). The spectral element method: An effective tool to simulate the seismic response of 2D and 3D geological structures, *Bull. Seismol. Soc. Am.* **88**, 368–392.
- Krebs, J. R., J. E. Anderson, D. Hinkley, R. Neelamani, S. Lee, A. Baumstein, and M. Lacasse (2009). Fast full-wavefield seismic inversion using encoded sources, *Geophysics* **74**, WCC177–WCC188.
- Krebs, J. R., Y. Cha, S. Lee, P. Dimitrov, A. Mullur, N. Downey, and P. Routh (2013). Orthogonal source and receiver encoding, *U.S. Patent Application (Patent 10,012,745)*.
- Krischer, L., A. Fichtner, S. Zukauskaitė, and H. Igel (2015). Large-scale seismic inversion framework, *Seismol. Res. Lett.* **86**, no. 4, 1198–1207, doi: [10.1785/0220140248](https://doi.org/10.1785/0220140248).
- Kustowski, B., G. Ekström, and A. M. Dziewoński (2008). Anisotropic shear-wave velocity structure of the Earth's mantle: A global model, *J. Geophys. Res.* **113**, no. B6, doi: [10.1029/2007JB005169](https://doi.org/10.1029/2007JB005169).
- Lailly, P. (1983). The seismic inverse problem as a sequence of before stack migration, in *Conference on Inverse Scattering: Theory and Application*, J. Bednar (Editor), SIAM, Philadelphia, 206–220.
- Laske, G., and G. Masters (1996). Constraints on global phase velocity maps from long-period polarization data, *J. Geophys. Res.* **101**, 16,059–16,075.
- Lau, H., J. Austermann, J. Mitrovica, O. Crawford, D. Al-Attar, and K. Latychev (2018). Inferences of mantle viscosity based on ice age datasets: The bias in radial viscosity profiles due to the neglect of laterally heterogeneous viscosity structure, *J. Geophys. Res.* **123**, 7237–7252.
- Lebedev, S., and G. Nolet (2003). Upper mantle beneath southeast Asia from S velocity tomography, *J. Geophys. Res.* **108**, doi: [10.1029/2000JB000073](https://doi.org/10.1029/2000JB000073).
- Lebedev, S., J. M.-C. Adam, and T. Meier (2013). Mapping the Moho with seismic surface waves: A review, resolution analysis, and recommended inversion strategies, *Tectonophysics* **609**, 377–394.
- Lebedev, S., J. Fullea, Y. Xu, and R. Bonadio (2024). Seismic thermography, *Bull. Seismol. Soc. Am.* doi: [10.1785/0120230245](https://doi.org/10.1785/0120230245).
- Lebedev, S., J. Grannell, P. Arroucau, R. Bonadio, N. P. Agostinetti, and C. J. Bean (2023). Seismicity of Ireland, and why it is so low: How the thickness of the lithosphere controls intraplate seismicity, *Geophys. J. Int.* **235**, no. 1, 431–447.
- Lei, W., Y. Ruan, E. Bozdağ, D. Peter, M. Lefebvre, D. Komatitsch, J. Tromp, J. Hill, N. Podhorszki, and D. Pugmire (2020). Global adjoint tomography—Model GLAD-M25, *Geophys. J. Int.* **223**, no. 1, 1–21, doi: [10.1093/gji/ggaa253](https://doi.org/10.1093/gji/ggaa253).
- Lekić, V., and B. Romanowicz (2011). Inferring upper-mantle structure by full waveform tomography with the spectral-element method, *Geophys. J. Int.* **185**, 799–831.
- Leng, K. D., J. Korenaga, and T. Nissen-Meyer (2020). 3-D scattering of elastic waves by small scale heterogeneities in the Earth's mantle, *Geophys. J. Int.* **223**, 502–525.
- Lêvêque, J. J., L. Rivera, and G. Wittlinger (1993). On the use of the checkerboard test to assess the resolution of tomographic inversions, *Geophys. J. Int.* **115**, 313–318.
- Li, X. B., and B. Romanowicz (1996). Global mantle shear velocity model developed using nonlinear asymptotic coupling theory, *J. Geophys. Res.* **101**, 11,245–22,271.
- Lin, F.-C., D. Li, R. W. Clayton, and D. Hollis (2013). High-resolution 3D shallow crustal structure in Long Beach, California: Application of ambient noise tomography on a dense seismic array, *Geophysics* **78**, Q45–Q56.
- Lin, F.-C., V. C. Tsai, and B. Schmandt (2014). 3-D crustal structure of the western United States: Application of Rayleigh-wave ellipticity extracted from noise cross-correlations, *Geophys. J. Int.* **198**, no. 2, 656–670.
- Liu, X. (2020). Finite-frequency sensitivity kernels for seismic noise interferometry based on differential time measurements, *J. Geophys. Res.* **125**, e2019JB018932, doi: [10.1029/2019JB018932](https://doi.org/10.1029/2019JB018932).

- Liu, Q., and Y. Gu (2012). Seismic imaging: From classical to adjoint tomography, *Tectonophysics* **566–567**, 31–66.
- Liu, Z., J. Hoffman, E. Bachmann, C. Cui, F. J. Simons, and J. Tromp (2024). Laplace domain crosstalk-free source-encoded elastic full waveform inversion using time domain solvers, *Geophysics* doi: [10.1190/geo2023-0351.1](https://doi.org/10.1190/geo2023-0351.1).
- Lv, M., X. Xu, S. Hu, Z. Ding, and P. Yao (2024). Crustal deformation in eastern Himalayan syntaxis constrained by ambient noise tomography, *Bull. Seismol. Soc. Am.* doi: [10.1785/0120230228](https://doi.org/10.1785/0120230228).
- Lyu, C., L. Zhao, Y. Capdeville, and Z. Wei (2024). Error propagation and control in 2D and 3D hybrid seismic wave simulations for box tomography, *Bull. Seismol. Soc. Am.* doi: [10.1785/0120230235](https://doi.org/10.1785/0120230235).
- Macchioli-Grande, F., F. Zyserman, L. Monachesi, L. Jouniaux, and M. Rosas-Carbajal (2020). Bayesian inversion of joint SH seismic and seismoelectric data to infer glacier system properties, *Geophys. Prospect.* **68**, no. 5, 1633–1656.
- Mahardika, H., A. Revil, and A. Jardani (2012). Waveform joint inversion of seismograms and electrograms for moment tensor characterization of fracking events, *Geophysics* **77**, no. 5, ID23–ID39.
- Mahesh, P., C. Sribin, P. Dewangan, V. Yatheesh, and S. Gupta (2024). 3-dimensional local earthquake tomography of the Andaman-Nicobar subduction zone using ocean bottom seismometer data, *Bull. Seismol. Soc. Am.* doi: [10.1785/0120230240](https://doi.org/10.1785/0120230240).
- Mancini, F., K. Prindle, T. Ridsdill-Smith, and J. Moss (2016). Full-waveform inversion as a game changer: Are we there yet? *Lead. Edge* **35**, no. 5, 445–451, doi: [10.1190/tle35050445.1](https://doi.org/10.1190/tle35050445.1).
- Marquering, H., F. Dahlen, and G. Nolet (1999). Three-dimensional sensitivity kernels for finite-frequency travel times: The banana-doughnut paradox, *Geophys. J. Int.* **137**, 805–815, doi: [10.1046/j.1365-246x.1999.00837.x](https://doi.org/10.1046/j.1365-246x.1999.00837.x).
- Martins Gomes, V. (2022). Experimental characterization and modelling of electromagnetic waves generated by seismoelectric conversion at porous media interfaces, *Theses*, Université de Pau et des Pays de l'Adour, available at <https://theses.hal.science/tel-04136776> (last accessed April 2024).
- Masson, Y. (2023). Distributional finite-difference modelling of seismic waves, *Geophys. J. Int.* **233**, 264–296.
- Masson, Y., and B. Romanowicz (2017). Box tomography: Localised imaging of remote targets buried in an unknown medium, a step forward for understanding key structures in the deep earth, *Geophys. J. Int.* **211**, 141–163.
- Maupin, V., and J. Park (2007). Wave propagation in anisotropic media, in *Seismology and Structure of the Earth*, B. Romanowicz and A. Dziewonski (Editors), Vol. 1, Elsevier, Amsterdam, The Netherlands, 289–321.
- McKenzie, D., J. Jackson, and K. Priestley (2005). Thermal structure of oceanic and continental lithosphere, *Earth Planet. Sci. Lett.* **233**, 337–349.
- McNamara, A. K. (2019). A review of large low shear velocity provinces and ultra low velocity zones, *Tectonophysics* **760**, 199–220.
- Mégnin, C., and B. Romanowicz (2000). The 3D shear velocity structure of the mantle from the inversion of body, surface and higher modes wave forms, *Geophys. J. Int.* **143**, 709–728.
- Meyer, R.-C. (2021). Mathematical modeling and simulation of waves in conducting poroelastic media using HDG method, *Theses*, Université de Pau et des Pays de l'Adour, available at <https://theses.hal.science/tel-03442300> (last accessed April 2024).
- Mikhailov, O. V., J. Queen, and M. N. Toksöz (2000). Using borehole electroseismic measurements to detect and characterize fractured (permeable) zones, *Geophysics* **65**, no. 4, 1098–1112.
- Modrak, R. T., D. Borisov, M. Lefebvre, and J. Tromp (2018). Seisflows—Flexible waveform inversion software, *Comput. Geosci.* **115**, 88–95, doi: [10.1016/j.cageo.2018.02.004](https://doi.org/10.1016/j.cageo.2018.02.004).
- Monteiller, V., S. Chevrot, D. Komatitsch, and N. Fuji (2013). A hybrid method to compute short-period synthetic seismograms of teleseismic body waves in a 3-D regional model, *Geophys. J. Int.* **192**, 230–247.
- Morency, C., and E. Matzel (2021). Seismic to electric conversion for carbon storage monitoring, *Sixth International Conference on Engineering Geophysics, Virtual*, 25–28 October 2021, 195–198.
- Morency, C., Y. Luo, and J. Tromp (2011). Acoustic, elastic and poroelastic simulations of CO₂ sequestration crosswell monitoring based on spectral-element and adjoint methods, *Geophys. J. Int.* **185**, 955–966.
- Morency, C., E. Matzel, N. Grobde, D. Brito, C. Bordes, N. Bernardo, H. Barucq, J. Diaz, A. Heta, M. Bellanger, *et al.* (2022). Seismoelectric effects for geothermal resources assessment and monitoring: Overview and preliminary results, *Proc. of the 47th Workshop on Geothermal Reservoir Engineering*, Stanford University, Stanford, California, 7–9 February 2022, SGP-TR-223 pp.
- Naif, S., K. Key, S. Constable, and R. L. Evans (2013). Melt-rich channel observed at the lithosphere-asthenosphere boundary, *Nature* **495**, 356–359.
- Nakata, N., J. P. Chang, J. F. Lawrence, and P. Boué (2015). Body wave extraction and tomography at Long Beach, California, with ambient-noise interferometry, *J. Geophys. Res.* **120**, 1159–1173.
- Neal, R. M. (2011). MCMC using Hamiltonian dynamics, in *Handbook of Markov Chain Monte Carlo*, S. Brooks, A. Gelman, G. Jones, and X.-L. Meng (Editors), Chapman and Hall, London, United Kingdom, 113–162.
- Nocedal, J., and S. J. Wright (1999). *Numerical Optimization*, Springer, New York.
- Nolet, G. (2008). *A Breviary of Seismic Tomography*, Cambridge University Press, Cambridge, United Kingdom.
- Nolet, G., and F. A. Dahlen (2000). Wavefront healing and the evolution of seismic delay times, *J. Geophys. Res.* **105**, 19,043–19,054.
- Nuzzo, R. (2014). Statistical errors, *Nature* **506**, 150–152.
- Nyblade, A. A., R. Durrheim, P. Dirks, G. Graham, R. Gibson, and S. Webb (2011). Geoscience initiative develops sustainable science in Africa, *Eos Trans. AGU* **92**, doi: [10.1029/2011E0190002](https://doi.org/10.1029/2011E0190002).
- Obayashi, M., J. Yoshimitsu, G. Nolet, Y. Fukao, H. Shiobara, H. Sugioka, H. Miyamachi, and Y. Gao (2013). Finite frequency whole mantle P wave tomography: Improvement of subducted slab images, *Geophys. Res. Lett.* **40**, no. 21, 5652–5657, doi: [10.1002/2013GL057401](https://doi.org/10.1002/2013GL057401).
- Okaya, D., W. Rabbel, T. Beilecke, and J. Hasenclever (2004). P wave material anisotropy of a tectono-metamorphic terrane: An active source seismic experiment at the KTB super-deep drill hole, southeast Germany, *Geophys. Res. Lett.* **31**, doi: [10.1029/2004GL020855](https://doi.org/10.1029/2004GL020855).
- Oldenburg, D. W. (1974). The inversion and interpretation of gravity anomalies, *Geophysics* **39**, 526–536.
- Park, S., J.-P. Avouac, Z. Zhan, and A. Gualandi (2023). Weak upper-mantle base revealed by postseismic deformation of a deep earthquake, *Nature* **615**, 455–460.

- Pavlis, G. L., and J. R. Booker (1980). The mixed discrete-continuous inverse problem: Application to the simultaneous determination of earthquake hypocenters and velocity structure, *J. Geophys. Res.* **85**, 4801–4810, doi: [10.1029/JB085iB09p04801](https://doi.org/10.1029/JB085iB09p04801).
- Pienkowska, M., V. Monteillier, and T. Nissen-Meyer (2021). High-frequency global wavefields for local 3-D structures by wavefield injection and extrapolation, *Geophys. J. Int.* **223**, 1782–1798.
- Pipatprathanporn, S., and F. J. Simons (2022). One year of sound recorded by a MERMAID float in the Pacific: Hydroacoustic earthquake signals and infrasonic ambient noise, *Geophys. J. Int.* **228**, 193–212, doi: [10.1093/gji/ggab296](https://doi.org/10.1093/gji/ggab296).
- Pladys, A., R. Brossier, Y. Li, and L. Metivier (2021). On cycle-skipping and misfit function modification for full-wave inversion: Comparison of five recent approaches, *Geophysics* **86**, R563–R587.
- Powell, E., N. Gomez, C. Hay, K. Latychev, and J. Mitrovica (2020). Viscous effects in the solid Earth response to modern Antarctic ice mass flux: Implications for geodetic studies of WAIS stability in a warming world, *J. Clim.* **33**, 443–459.
- Pride, S. R. (1994). Governing equations for the coupled electromagnetics and acoustics of porous media, *Phys. Rev. B* **50**, 15,678–15,696.
- Priestley, K., T. Ho, Y. Takei, and D. McKenzie (2024). The thermal and anisotropic structure of the top 300 km of the mantle, *Earth Planet. Sci. Lett.* **626**, doi: [10.1016/j.epsl.2023.118525](https://doi.org/10.1016/j.epsl.2023.118525).
- Priestley, K., and D. McKenzie (2006). The thermal structure of the lithosphere from shear wave velocities, *Earth Planet. Sci. Lett.* **244**, 285–301.
- Priestley, K., and D. McKenzie (2013). The relationship between shear wave velocity, temperature, attenuation and viscosity in the shallow part of the mantle, *Earth Planet. Sci. Lett.* **381**, 78–91.
- Quarteroni, A., A. Manzoni, and F. Negri (2016). *Reduced Basis Methods for Partial Differential Equations: An Introduction*, Springer, Cham, Switzerland.
- Resovsky, J., and J. Trampert (2002). Reliable mantle density error bars: An application of the Neighbourhood Algorithm to normal-mode and surface wave data, *Geophys. J. Int.* **150**, no. 3, 665–672.
- Revil, A., and A. Jardani (2010). Seismoelectric response of heavy oil reservoirs: Theory and numerical modelling, *Geophys. J. Int.* **180**, 781–797.
- Ringler, A. T., R. E. Anthony, R. C. Aster, C. J. Ammon, S. Arrowsmith, H. Benz, C. Ebeling, A. Frassetto, W. Y. Kim, P. Koelemeijer, et al. (2022). Achievements and prospects of global broadband seismographic networks after 30 years of continuous geophysical observations, *Rev. Geophys.* **60**, doi: [10.1029/2021RG000749](https://doi.org/10.1029/2021RG000749).
- Ritsema, J., and V. Lekić (2020). Heterogeneity of seismic wave velocity in Earth's mantle, *Annu. Rev. Earth Planet. Sci.* **48**, 377–401, doi: [10.1146/annurev-earth-082119-065909](https://doi.org/10.1146/annurev-earth-082119-065909).
- Ritsema, J., and H. J. van Heijst (2002). Constraints on the correlation of P- and S-wave velocity heterogeneity in the mantle from P, PP, PPP and PKPab traveltimes, *Geophys. J. Int.* **149**, 482–489.
- Ritsema, J., L. A. Rivera, D. Komatitsch, J. Tromp, and H.-J. van Heijst (2002). Effects of crust and mantle heterogeneity on pp/p and ss/s amplitude ratios, *Geophys. Res. Lett.* **29**, no. 10, 72-1–72-4, doi: [10.1029/2001GL013831](https://doi.org/10.1029/2001GL013831).
- Robertson, G. S., and J. H. Woodhouse (1996). Ratio of relative S to P velocity heterogeneity in the lower mantle, *J. Geophys. Res.* **101**, doi: [10.1029/96JB01905](https://doi.org/10.1029/96JB01905).
- Robson, A., H. C. P. Lau, P. Koelemeijer, and B. Romanowicz (2022). An analysis of core-mantle boundary Stoneley mode sensitivity and sources of uncertainty, *Geophys. J. Int.* **228**, 1962–1974, doi: [10.1093/gji/ggab448](https://doi.org/10.1093/gji/ggab448).
- Rodgers, A., L. Krischer, A. Afanasiev, C. Boehm, C. Doody, and N. Simmons (2024). Adjoint waveform tomography for crustal and upper mantle structure of the Middle East and Southwest Asia for improved waveform simulations using openly available broadband data, *Bull. Seismol. Soc. Am.* doi: [10.1785/0120230248](https://doi.org/10.1785/0120230248).
- Rodgers, A., L. Krischer, M. Afanasiev, C. Boehm, C. Doody, A. Chiang, and N. Simmons (2022). WUS256: An adjoint waveform tomography model of the crust and upper mantle of the western United States for improved waveform simulations, *J. Geophys. Res.* **127**, no. 7, e2022JB024549, doi: [10.1029/2022JB024549](https://doi.org/10.1029/2022JB024549).
- Romanowicz, B. (2023). Global seismic tomography using time-domain waveform inversion, in *Applications of Data Assimilation and Inverse Problems in the Earth Sciences*, Cambridge University Press, Cambridge, United Kingdom, 220–234.
- Romanowicz, B., and B. J. Mitchell (2015). Deep earth structure—Q of the earth from crust to core, in *Treatise on Geophysics*, A. Dziewonski and B. Romanowicz (Editors), Elsevier, Amsterdam, The Netherlands, 789–827.
- Romero, L., D. Ghiglia, C. Ober, and S. Morton (2000). Phase encoding of shot records in prestack migration, *Geophysics* **65**, 426–436.
- Rozza, G., D. Huynh, and A. Patera (2008). Reduced basis approximation and a posteriori error estimation for affinely parametrized elliptic coercive partial differential equations: Application to transport and continuum mechanics, *Arch. Comput. Meth. Eng.* **15**, 229–275.
- Sager, K., C. Boehm, L. Ermert, L. Krischer, and A. Fichtner (2020). Global-scale full-waveform ambient noise inversion, *J. Geophys. Res.* **125**, doi: [10.1029/2019JB018644](https://doi.org/10.1029/2019JB018644).
- Sambridge, M. S., K. Gallagher, A. Jackson, and P. Rickwood (2006). Transdimensional inverse problems, model comparison, and the evidence, *Geophys. J. Int.* **167**, 528–542.
- Santosa, F., and W. W. Symes (1988). Computation of the Hessian for least-squares solutions of inverse problems of reflection seismology, *Inverse Prob.* **4**, 211–233.
- Schiemenz, A., and H. Igel (2013). Accelerated 3-D full-waveform inversion using simultaneously encoded sources in the time domain: Application to Valhall ocean-bottom cable data, *Geophys. J. Int.* **195**, 1970–1988.
- Schuster, G., X. Wang, Y. Huang, W. Dai, and C. Boonyasriwat (2011). Theory of multisource crosstalk reduction by phase-encoded statics, *Geophys. J. Int.* **184**, 1289–1303.
- Shinevar, W. J., E. M. Golos, O. Jagoutz, M. D. Behn, and R. D. van der Hilst (2023). Mantle thermochemical variations beneath the continental United States through petrologic interpretation of seismic tomography, *Earth Planet. Sci. Lett.* **602**, 117965, doi: [10.1016/j.epsl.2022.117965](https://doi.org/10.1016/j.epsl.2022.117965).
- Shinevar, W. J., O. Jagoutz, and M. D. Behn (2022). WISTFUL: Whole-rock interpretative seismic toolbox for ultramafic lithologies, *Geochem. Geophys. Geosys.* **23**, no. 8, e2022GC010329, doi: [10.1029/2022GC010329](https://doi.org/10.1029/2022GC010329).
- Sieminski, A., J. Trampert, and J. Tromp (2009). Principal component analysis of anisotropic finite-frequency kernels, *Geophys. J. Int.* **179**, 1186–1198.

- Simons, F. J., J. D. Simon, and S. Pipatprathanporn (2021). Twenty-thousand leagues under the sea: Recording earthquakes with autonomous floats, *Acous. Today* **17**, no. 2, 42–51.
- Spencer, C., and D. Gubbins (1980). Travel-time inversion for simultaneous earth-quake location and velocity structure determination in laterally varying media, *Geophys. J. Int.* **63**, 95–116, doi: [10.1111/j.1365-246X.1980.tb02612.x](https://doi.org/10.1111/j.1365-246X.1980.tb02612.x).
- Spetzler, J., and R. Snieder (2001). The effect of small scale heterogeneity on the arrival time of waves, *Geophys. J. Int.* **145**, 786–796.
- Staebler, S. C., K. Sigloch, and T. Nissen-Meyer (2012). Triplicated P-wave measurements for waveform tomography of the mantle transition zone, *Solid Earth* **3**, doi: [10.5194/se-3-339-2012](https://doi.org/10.5194/se-3-339-2012).
- Stanzione, D., J. West, R. Evans, T. Minyard, O. Ghattas, and D. Panda (2020). Frontera: The evolution of leadership computing at the national science foundation, *Practice and Experience in Advanced Research Computing*, 106–111, doi: [10.1145/3311790.3396656](https://doi.org/10.1145/3311790.3396656).
- Suetsugu, D., and H. Shiobara (2014). Broadband ocean bottom seismology, *Annu. Rev. Earth Planet. Sci.* **42**, 27–43.
- Sukhovich, A., S. Bonnioux, Y. Hello, J.-O. Irisson, F. Simons, and G. Nolet (2015). Long-awaited mathematics proof could help scan Earth's innards, *Nat. Commun.* **6**, 8027–8033.
- Tanaka, H. K. M., T. Uchida, M. Tanaka, H. Shinohara, and H. Taira (2009). Cosmic-ray muon imaging of magma in a conduit: Degassing process of Satsuma-Iwojima volcano, Japan, *Geophys. Res. Lett.* **36**, L01304, doi: [10.1029/2008GL036451](https://doi.org/10.1029/2008GL036451).
- Tao, K., S. P. Grand, and F. Niu (2018). Seismic structure of the upper mantle beneath eastern Asia from full waveform seismic tomography, *Geochem. Geophys. Geosys.* **19**, no. 8, 2732–2763, doi: [10.1029/2018GC007460](https://doi.org/10.1029/2018GC007460).
- Tape, W., and C. Tape (2022). Two complementary methods of inferring elastic symmetry, *J. Elasticity* **150**, 91–118, doi: [10.1007/s10659-022-09898-0](https://doi.org/10.1007/s10659-022-09898-0).
- Tape, C., Q. Liu, A. Maggi, and J. Tromp (2009). Adjoint tomography of the southern California crust, *Science* **325**, 988–992.
- Tape, C., Q. Liu, A. Maggi, and J. Tromp (2010). Seismic tomography of the southern California crust based upon spectral-element and adjoint methods, *Geophys. J. Int.* **180**, 433–462.
- Tarantola, A. (1984). Inversion of seismic reflection data in the acoustic approximation, *Geophysics* **49**, no. 8, 1259–1266.
- Tarantola, A., and B. Valette (1982). Generalized nonlinear inverse problems solved using the least squares criterion, *Rev. Geophys.* **20**, 219–232.
- Thompson, A. H., and G. A. Gist (1993). Geophysical applications of electrokinetic conversion, *Lead. Edge* **12**, 1169–1173.
- Thrustarson, S., M. van Driel, L. Krischer, C. Boehm, M. Afanasiev, D.-P. van Herwaarden, and A. Fichtner (2020). Accelerating numerical wave propagation by wavefield adapted meshes, Part II: Full-waveform inversion, *Geophys. J. Int.* **221**, 1591–1604.
- Thrustarson, S., D.-P. van Herwaarden, L. Krischer, and A. Fichtner (2021). LASIF: Large-Scale Seismic Inversion Framework: An updated version, *Earth ArXiv*, doi: [10.31223/X5NC84](https://doi.org/10.31223/X5NC84).
- Thrustarson, S., D.-P. van Herwaarden, S. Noe, C. Schiller, and A. Fichtner (2024). REVEAL: A global full-waveform inversion model, *Bull. Seismol. Soc. Am.* doi: [10.5281/zenodo.10684325](https://doi.org/10.5281/zenodo.10684325).
- Thurber, C., and D. Eberhart-Phillips (1999). Local earthquake tomography with flexible gridding, *Comput. Geosci.* **25**, 809–818, doi: [10.1016/S0098-3004\(99\)00007-2](https://doi.org/10.1016/S0098-3004(99)00007-2).
- Tong, P., C. W. Chen, D. Komatitsch, P. Basini, and Q. Y. Liu (2014). High resolution seismic array imaging based on an SEM-FK hybrid method, *Geophys. J. Int.* **197**, no. 1, 369–395.
- Tromp, J. (2020). Seismic wavefield imaging of Earth's interior across scales, *Nat. Rev. Earth Environ.* **1**, 40–53, doi: [10.1038/s43017-019-0003-8](https://doi.org/10.1038/s43017-019-0003-8).
- Tromp, J., and E. Bachmann (2019). Source encoding for adjoint tomography, *Geophys. J. Int.* **218**, 2019–2044.
- Tromp, J., C. Tape, and Q. Liu (2005). Seismic tomography, adjoint methods, time reversal and banana-doughnut kernels, *Geophys. J. Int.* **160**, 195–216, doi: [10.1111/j.1365-246X.2004.02453.x](https://doi.org/10.1111/j.1365-246X.2004.02453.x).
- Tsai, V. C. (2023). The future of Earth imaging, *Seismol. Res. Lett.* **94**, 2119–2128, doi: [10.1785/0220230125](https://doi.org/10.1785/0220230125).
- Tsai, V. C., C. Huber, and C. A. Dalton (2023). Towards the geological parametrization of seismic tomography, *Geophys. J. Int.* **234**, 1447–1462, doi: [10.1093/gji/ggad140](https://doi.org/10.1093/gji/ggad140).
- Tshekmistrenko, M., K. Sigloch, K. Hosseini, and G. Barruol (2021). A tree of Indo-African mantle plumes imaged by seismic tomography, *Nature Geosci.* **14**, doi: [10.1038/s41561-021-00762-9](https://doi.org/10.1038/s41561-021-00762-9).
- van der Wal, W., P. L. Whitehouse, and E. J. Schrama (2015). Effect of GIA models with 3D composite mantle viscosity on GRACE mass balance estimates for Antarctica, *Earth Planet. Sci. Lett.* **414**, 134–143.
- van Herwaarden, D.-P., C. ehmvBo, M. Afanasiev, S. Thrustarson, L. Krischer, M. van Driel, and A. Fichtner (2020). Accelerated full-waveform inversion using dynamic mini-batches, *Geophys. J. Int.* **221**, 1427–1438.
- Vehtari, A., A. Gelman, and J. Gabry (2017). Practical Bayesian model evaluation using leave-one-out cross validation and WAIC, *Stat. Comput.* **27**, 1413–1432.
- Virieux, J., and S. Operto (2009). An overview of full-waveform inversion in exploration geophysics, *Geophysics* **74**, WCC1–WCC26.
- Virieux, J., A. Asnaashari, R. Brossier, L. Metivier, A. Ribodetti, and W. Zhou (2017). An introduction to full-waveform inversion, *Encyclopedia of Exploration Geophysics*, doi: [10.1190/1.9781560803027.entry6](https://doi.org/10.1190/1.9781560803027.entry6).
- Volterra, V. (2005). *Theory of Functionals and of Integral and Integro-Differential Equations*, Dover Publications, New York.
- Wang, K., Q. Liu, and Y. Yang (2019). Three-dimensional sensitivity kernels for multicomponent empirical Green's functions from ambient noise: Methodology and application to adjoint tomography, *J. Geophys. Res.* **124**, 5794–5810, doi: [10.1029/2018JB017020](https://doi.org/10.1029/2018JB017020).
- Wang, K., Y. J. Yang, C. X. Jiang, Y. Wang, P. Tong, T. S. Liu, and Q. Y. Liu (2021). Adjoint tomography of ambient noise data and teleseismic P waves: Methodology and applications to central California, *J. Geophys. Res.* **126**, no. 6, e2021JB021648, doi: [10.1029/2021JB021648](https://doi.org/10.1029/2021JB021648).
- Wang, Y., S. Chevrot, V. Monteiller, D. Komatitsch, F. Mouthereau, G. Manatschal, M. Sylvander, J. Diaz, M. Ruiz, F. Grimaud, et al. (2016). The deep roots of the western Pyrenees revealed by full waveform inversion of teleseismic P waves, *Geology* **44**, 475–478.
- Wang, Y., F.-C. Lin, and K. M. Ward (2019). Ambient noise tomography across the cascadia subduction zone using dense linear seismic arrays and double beamforming, *Geophys. J. Int.* **217**, no. 3, 1668–1680.
- Wasserstein, R. L., and N. A. Lazar (2016). The ASA's statement on p-values: Context, process, and purpose, *Am. Stat.* **70**, 129–133.

- Widmer, R., G. Masters, and F. Gilbert (1991). Spherically symmetric attenuation within the Earth from normal mode data, *Geophys. J. Int.* **104**, 541–553.
- Wilgus, J., B. Schmandt, R. Maguire, C. Jiang, and J. Chaput (2023). Shear velocity evidence of upper crustal magma storage beneath valles caldera, *Geophys. Res. Lett.* **50**, no. 5, e2022GL101520, doi: [10.1029/2022GL101520](https://doi.org/10.1029/2022GL101520).
- Woodhouse, J. H., and A. M. Dziewoński (1984). Mapping the upper mantle: Three-dimensional modeling of Earth structure by inversion of seismic waveforms, *J. Geophys. Res.* **89**, 5953–5986, doi: [10.1029/JB089iB07p05953](https://doi.org/10.1029/JB089iB07p05953).
- Woodhouse, J. H., and Y. Wong (1986). Amplitude, phase and path anomalies of mantle waves, *Geophys. J. Roy. Astron. Soc.* **87**, 753–773.
- Xu, M. J., K. Wang, J. Chen, D. Y. Yu, and P. Tong (2023). Three-dimensional receiver function adjoint tomography for high-resolution seismic array imaging: Methodology and applications in southeastern Tibet, *J. Geophys. Res.* doi: [10.21979/N9/MBWEP5](https://doi.org/10.21979/N9/MBWEP5).
- Yang, X., and H. Gao (2020). Segmentation of the Aleutian-Alaska subduction zone revealed by full-wave ambient noise tomography: Implications for the along-strike variation of volcanism, *J. Geophys. Res.* **125**, no. 11, e2020JB019677, doi: [10.1029/2020JB019677](https://doi.org/10.1029/2020JB019677).
- Yang, Y., and B. Engquist (2018). Analysis of optimal transport and related misfit functions in full-waveform inversion, *Geophysics* **83**, A7–A12.
- Yoshizawa, K., and B. L. N. Kennett (2002). Determination of the influence zone for surface wave paths, *Geophys. J. Int.* **149**, 440–453.
- Yuan, S., and W. Xu (2019). The new progress of China Array project, *Geophys. Res. Abstr. EGU General Assembly*, 21, Vienna, Austria, 7–12 April 2019, available at <https://meetingorganizer.copernicus.org/EGU2019/EGU2019-180> (last accessed April 2024).
- Yuan, Y. O., F. J. Simons, and J. Tromp (2016). Double-difference adjoint seismic tomography, *Geophys. J. Int.* **206**, 1599–1618, doi: [10.1093/gji/ggw233](https://doi.org/10.1093/gji/ggw233).
- Zenonos, A., L. De Siena, S. Widiyantoro, and N. Rawlinson (2019). P and S wave travel time tomography of the SE Asia-Australia collision zone, *Phys. Earth Planet. In.* **293**, 106267, doi: [10.1016/j.pepi.2019.05.010](https://doi.org/10.1016/j.pepi.2019.05.010).
- Zhang, H., and C. Thurber (2003). Double-difference tomography: The method and its application to the Hayward fault, California, *Bull. Seismol. Soc. Am.* **93**, 1875–1889, doi: [10.1785/0120020190](https://doi.org/10.1785/0120020190).
- Zhang, X., and A. Curtis (2020). Seismic tomography using variational inference methods, *J. Geophys. Res.* **125**, no. 4, e2019JB018589, doi: [10.1029/2019JB018589](https://doi.org/10.1029/2019JB018589).
- Zhang, Q., W. Mao, H. Zhou, H. Zhang, and Y. Chen (2018). Hybrid-domain simultaneous-source full waveform inversion without crosstalk noise, *Geophys. J. Int.* **215**, 1659–1681.
- Zhang, X., A. Lomas, M. Zhou, Y. Zheng, and A. Curtis (2022). 3-D Bayesian variational full waveform inversion, *Geophys. J. Int.* **234**, 546–561.
- Zhao, D., J. Wang, Z. Huang, and X. Liu (2021). Seismic structure and subduction dynamics of the western Japan arc, *Tectonophysics* **802**, 228743, doi: [10.1016/j.tecto.2021.228743](https://doi.org/10.1016/j.tecto.2021.228743).
- Zhao, L., T. H. Jordan, and C. H. Chapman (2000). Three-dimensional Fréchet differential kernels for seismic delay times, *Geophys. J. Int.* **141**, 558–576, doi: [10.1046/j.1365-246x.2000.00085.x](https://doi.org/10.1046/j.1365-246x.2000.00085.x).
- Zhao, Z., M. Sen, and P. Stoffa (2016). Double-plane-wave reverse time migration in the frequency domain, *Geophysics* **81**, no. 5, S367–S382.
- Zhou, Z., P. Gerstoft, and K. B. Olsen (2024). 3D multiresolution velocity model fusion with probability graphical models, *Bull. Seismol. Soc. Am.* doi: [10.1785/0120230271](https://doi.org/10.1785/0120230271).
- Zhu, H., E. Bozdağ, and J. Tromp (2015). Seismic structure of the European upper mantle based on adjoint tomography, *Geophys. J. Int.* **201**, no. 1, 18–52.

Manuscript received 14 September 2023
Published online 3 May 2024